7-5-2017

Novel Approaches to the Spectral and Colorimetric Color Reproduction

Morteza Maali Amiri
mm2391@rit.edu

R·I·T

Novel Approaches to the Spectral and Colorimetric Color Reproduction

by

Morteza Maali Amiri

A Thesis Submitted in Partial Fulfillment of the
Requirements for the Degree of Masters of Science
in Color Science

Program of Color Science
College of Science
Rochester Institute of Technology
Rochester, NY

July 5, 2017

Signature of Author _____

Accepted by _____
Dr. Mark Fairchild, Graduate Program Director Date

COLLEGE OF SCIENCE

ROCHESTER INSTITUTE OF TECHNOLOGY

ROCHESTER, NEW YORK

CERTIFICATE OF APPROVAL

MASTERS DEGREE THESIS

The Masters Degree Thesis of Morteza Maali Amiri

Has been examined and approved by the

Committee as satisfactory for the

Thesis required for the

Masters degree in Color Science

_____

Dr. Mark D. Fairchild, Advisor

_____

Dr. Susan Farnand

_____

Date

THESIS RELEASE PERMISSION

ROCHESTER INSTITUTE OF TECHNOLOGY

PROGRAM OF COLOR SCIENCE

Title of Thesis:

Novel Approaches to the Spectral and Colorimetric Color Reproduction

I, Morteza Maali Amiri, hereby grant permission to Wallace Memorial Library of R.I.T. to reproduce my thesis in whole or in part. Any reproduction will not be for commercial use or profit.

Signature _____

Date

Abstract

All the different approaches taken for spectral data acquisition can be narrowed down to two main methods; the first one is using spectrophotometer, spectroradiometer, hyper- and multi- spectral camera through which the spectra can be most probably attained with a high level of accuracy in a direct manner. Nonetheless, the price at which the spectra are acquired is very high. However, there is also a second approached in which the spectra are estimated from the colorimetric information. The second approach, even though it is very cost efficient, is of limited level of accuracy, which could be due to the methods or the dissmiliarity of learning and testing samples used. In this work, through looking upon the spectral estimation in a different way, it is attempted to enhance the accuracy of the spectral estimation procedures which is fulfilled by associating the spectral recovery process with spectral sensitivity variability present in both different human observers and RGB cameras.

The work is split into two main sections, namely, theory and practice. In the first section, theory, the main idea of the thesis is examined through simulation, using different observers' color matching functions (CMFs) obtained from Asano's vision model and also different cameras' spectral sensitivities obtained from an open database. The second part of the work is concerned with putting the major idea of the thesis into use and is comprised of three subsections itself. In the first subsection, real cameras and cellphones are used. In the second subsection, using weighted regression, the idea presented in this work, is extended to a series of studies in which spectra are estimated from their corresponding CIEXYZ tristimulus values. In the last subsection, obserevers' colorimetric responses are simulated using color matching. Finally, it is shown that the methods presented in this work have a great potential to even rival multi-spectral cameras, whose equipment could be as expensive as a spectrophotometer.

Acknowledgements

I would like to express my gratitude to my advisor, Prof. Mark D. Fairchild, for his guidance, advice, and patience throughout this process. It was a great honor for me working with him and I have learnt a lot of things, apart from color science related topics, from him.

I would like to thank my family, my twin brother, Mojtaba and his girlfriend Evylin, my Mother, Sedigheh, my father, Motalleb, my oldest sister, Fatemeh, and my other siblings, Mahdi, Hadi, and Zakie for simply being who they are.

I would also like to thank my friends, Kamran Binaee, Farhad Abed, and Shahram Peyvandi for their advice and support throughout the program.

I would like to express my thanks to my RIT cohort, Gaurav Sheth, and Katey Carpenter.

I would like to thank Prof. Roy Berns, Dr. Susan Farnand, Dr. David Wyble, and Dr. Michael Murdoch, for sharing their knowledge and time with me over these past few years.

I would like to thank Valerie Hemink for her constant help and encouragement.

I would like to thank my advisor back in Iran, Prof. Amirshahi, for always advising and supporting me.

I would like to thank my friends, Aidin and his wife, Tuba and also Hossein and his wife, Shahnaz for introducing me to Christ and sharing with me their happiness.

I would also like to thank my friends, Sandy and her husband, Phil, who treat me the same as their own children and aid me in getting to know American cultures better.

Last but certainly not the least, I would like to express my thanks to my love, Carla, whose presence helps me overcome hardships more easily and replace my loneliness with love and joy.

Contents

List of Figures

List of Tables

1. Introduction

There has been many different methods for acquiring the spectral reflectance of a surface color; however, all these different approaches can be narrowed down to two major methods; using spectrophotometer, spectroradiometer, hyper-spectral camera and so forth is the first method that would enable direct access to spectral reflectance of objects. The obtained reflectance is of high accuracy; nonetheless, the high price of this approach could pose an impediment. Coming up with some kind of estimation in which the spectra are recovered from their corresponding colorimetric information is the second method. The low price of the second method is very intriguing but the low accuracy by which the spectra are estimated is not so intersting. Therefore, in this thesis, it is attempted to combine the positive features of the prior methods, i.e., high accuracy and low price, through looking upon the spectral recovery process in a different manner. In order to do that, the spectral sensitivity variability is associated with the spectral recovery process. To clarify, humans' and cameras' spectral sensitivity variability is described and connected to spectral sensitivity variability which is explained in more detail in the following sections.

People are not the same in color vision; it is not only limited to color deficiency but there is also a substantial difference between people possessing normal color vision [1]. Color matching functions (CMFs), which are fundamentally a set of 3 spectral sensitivity functions have the capability of characterization of human color vision. Therefore, human vision variability equates to that of CMFs. CMFs can be specified by the characteristics of lens, macular and three kinds of photo-pigments, L-, M- and S-, each having inter-observer variability, contributing their own specific variability to the total CMFs variability [2].

Prediction of color matches, and also ranges of matches, between individual with normal color vision under a specific viewing condition is possible through an individual observer's vision model. Nevertheless, most of the proposed, and so far utilized, models of vision are on the basis of average observer functions such as CIE 1931 and 1964 standard observers, and CIE 2006 Physiological Observer (CIEPO06) [3]. CIEPO06 specifies the average CMFs for the specific field size and age though utilization of two inputs, namely, field size and age. Moreover, in 1989 CIE proposed the standard deviate observer; although at first it seemed very promising, it was shown that it under-predict the observer variability in a significant manner.

Fairchild was the first to suggest utilizing Monte Carlo simulation to predict the normal vision individual CMFs [5]. The model was extended later by Fairchild and Heckaman using such physiological parameters as lens, macular pigment density and λ_{max} shifts of L- and M- cones as inputs [6, 7]. Some other researchers, on the other hand, have come up with different ideas trying to deal with the observers' vision variability; Sarkar and Blonde, as a case in point, mentioning the CMFs variability between different observers which results in mismatch among observers, devised the concept of colorimetric observer categories. Each category represents a different colorimetric observer subpopulation. Afterwards, they came up with a workflow reproducing colors on device on the basis of the observer's category. Their method is also known as personalized color reproduction. The most recent model of vision is devised by Asano et al. [9]. They devised a model taking in ten parameters as inputs enabling it to precisely predict the observers' CMFs variability. Visual angle and age, inherited from CIEPO06, are two of the inputs. Pigment density of the lens, deviation from average for peak optical density of macular pigment, deviation

from average for peak optical density of L-, M-, and S- photopigments, and deviation from average for L-, M- and S- photopigment λ_{max} shifts were the other eight physiological parameters used as inputs. The proposed model employs Monte Carlo in order to generate the CMFs of a color-normal population. To clarify, CIEPO06 would set the baseline and the suggested model deviates the baseline utilizing the eight physiological parameters.

Skimming through the above research papers would make one wonder whether putting a figure on vision variability between different people is helpful or not. There are two positive and negative aspects to CMF variability among different observers; in order to exactly match color for everyone their own particular set of CMFs should be used. This process would be very expensive considering now that the CIE 1931 and 1964 standard observers have been established and utilized for all the color reproduction algorithms. This, however, would remind us of the negative aspect of the CMFs variability. In this paper, it is attempted to unveil a positive aspect of CMFs variability among different observers through relating that to the spectral reflectance recovery process.

Accessing spectral data, which is regarded as the fingerprint of object, can specify color of the surface under different illuminations. Also, some algorithms of the color reproduction need spectral information [10]. Even though the spectral information can be very useful, they are not always available. However, their corresponding nonstandard colorimetric information (or color related information such as RGB, as opposed to the spectral ones) could be easily accessed using a camera or other color reproduction systems that are not as costly. Attaining the colorimetric data (, e.g., CIEXYZ tristimulus values) from the spectral information is readily performed; the reverse process, however, calculating the reflectance

spectra from the colorimetric data, is an ill-posed problem and consequently requires a more complex routine.

Thus, recovering the reflectance spectra from their colorimetric data has drawn a great level of attention, and has been the aim of numerous different scientific studies [10-18]. Owing to the fact that the spectral reflectance of non-fluorescent objects is ordinarily a smooth function of wavelength, a majority of the approaches up until now have employed linear models that are mostly based on Principal Component Analysis (PCA) [19-21]. Additionally, innumerable modifications has been made to PCA trying to improve the accuracy of the reconstruction [21-23]; it has been demonstrated, for example, that utilization of CIEXYZ captured under different illuminant types enhances the recovery accuracy in a significant manner [23]. Many other methods than PCA in conjunction with their modified versions have also received attention, such as interpolation, non-negative matrix factorization (NNMF), pseudo-inverse [24-26].

Most research papers in the area of the spectral recovery from the color related information have used CIEXYZ tristimulus values as their colorimetric data; however, there has been an interest in recovering the spectra from the RGB response of the cameras as well. They are of keen interest in that they use RGB color space of cameras, which is not standardized the way CIEXYZ is. It has been shown that utilizing different types of colored filters put in front of the camera could significantly improve the accuracy of the recovery process [27]. This situation can be likened to using different light sources in order to obtain a bigger matrix of colorimetric information.

Using multi-spectral cameras has also become customary using which the image of object is captured through at least seven filters that are placed in front of a monochrome sensor;

in other words, the camera is a seven or multi-channel camera as opposed to an ordinary RGB camera with only three channels. Use of this type of imaging device results in a far more accurate spectral reconstruction in comparison to the ordinary RGB cameras. Nonetheless, the price at which the equipment necessary for multi-spectral camera are acquired can be as high as a spectrophotometers.

In this work, the spectral recovery process is approached differently. Using different colorimetric data captured under different illumination types, or using colored filters in front of cameras makes one notice that accessing a larger set of colorimetric data of one specific object might aid in reconstructing the reflectance spectra. However, there are other ways to increase the colorimetric data dimensionality. As mentioned at the beginning of the introduction, observers are not similar when it comes to their visual capability, each of whom sees the world in their own specific manner. To clarify, if colorimetric information attained from different observers are put into use, there will be more colorimetric data for the object enabling a more accurate estimation of the spectral data. In this work, the spectral recovery process is looked upon differently; first it is shown how CMFs variability between different observers can help recover the reflectance better. After that, the same thing is done on camera, meaning the spectral sensitivity variability of different kinds of cameras are obtained and used in spectral reconstruction. Then, the same concept is applied to the real situation in which real smartphones and cameras are employed. Simulating observers' colorimetric response using regression and color matching is also presented. Finally, comparing the results of the above methods with multi-spectral cameras is done to reveal the potential of the approaches presented.

2. Literature Review

In this section some of the relevant papers are presented regarding the vision model, spectral recovery from CIEXYZ tristimulus values, spectral and color reproduction using RGB cameras and spectral color reproduction using multi-spectral cameras.

2.1. Vision Models

As mentioned in the introduction, after developing 1931 and 1964 standard observers it was realized that they might not be able to represent any real individulas. Because in both of the experiments in which these standard obsersers'sensitivities were determined a small number of observers were used and the results were averaged at the end. Standard deviate observer, on the other hand, even though it would show variability in different observers' CMFs, under-predicted the variability present in different observers' vision. It was then attempted to combine the observer variability model with psychophysical, physiological and genetics research. In this regard, cone fundamentals for mean observers with a particular age ranging from 20 to 80, and a field size of 1-10 degrees is computed. This process is what is used in CIEPO06. It does not take into account individuals' variability but only determines mean color matching functions for a specific field size and age. The procedure of CIEPO06 starts off by calculating the macular pigment maximum density as a function of field size. This is then utilized to scale a determined relative spectral density for macula. After that, the lens spectral optical density and other ocular media is calculated as a two-part age function. Also, the low-optical density absorbance spectra of the cone photopigments are derived and scaled by the peak visual pigment densities, which are field size functions, to attain the absorbance spectra of cones. At the end, the absorbance spectra

of cones are multiplied by the macular and ocular media transmittance leading to cone fundamentals [28]. The equations used in CIEPO06 would be presented in the next vision model presented by Asano et al.

Asano et al. have come up with the latest vision model taking into account the individuals' variability. Basically, the model proposed by Asano and his colleagues is defined as follows:

$$\text{Lms-CMFs} = f(a, v, d_{lens}, d_{macula}, d_L, d_M, d_S, s_L, s_M, s_s) \quad (1)$$

where, a is the subject's age, v denotes the visual angle, d_{lens} marks the deviation from average for lens pigment density, d_{macula} shows the deviation from average for macular pigment optical density, d_L, d_M and d_S denote the deviations from averages for L-, M-, and S- cone peak optical densities, respectively, s_L, s_M and s_s are deviations from average for L-, M- and S- cone λ_{max} shifts. Consequently, the basic inputs (forming the baseline, which are inherited from CIEPO06) to equation (1) are a and v. Now that some idea is obtained about the baseline of the model devised by Asano et al., the physiological parameters used by them are introduced in order to deviate this baselines.

Lens and other ocular media average spectral optical density, $D_{ocul,ave}(\lambda)$, can be attained for a subject aged between 20 and 60 (equation 2), and also for a subject aged over 60 (equation 3) as follows;

$$D_{ocul,ave}(\lambda) = D_{ocul,1}(\lambda)(1+0.02(a-32)) + D_{ocul,2}(\lambda) \quad (2)$$

$$D_{ocul,ave}(\lambda) = D_{ocul,1}(\lambda)(1.56+0.0667(a-60)) + D_{ocul,2}(\lambda) \quad (3)$$

where, $D_{ocul,1}$ denotes the portion that is influenced by aging, and $D_{ocul,2}$ marks the portion being independent of aging, which were derived by Pokorny et al.[13] Lens and other ocular media spectral optical density can be attained using the equation 4;

$$D_{ocul}(\lambda) = D_{ocul,ave}(\lambda)\ (1+(d_{lens}\ /100)) \quad (4)$$

The macular pigment optical density $D_{macula}(\lambda)$, can be obtained through the following equation:

$$D_{macula}(\lambda) = D_{max,macula} D_{relative,macula}(\lambda) \quad (5)$$

$$D_{max,macula} = 0.485e^{-v/6.132}(1+d_{macula}/100) \quad (6)$$

where, $D_{max,macula}$ represents the macular pigment peak optical density, and $D_{relative,macula}$ denotes the macular pigment relative optical density.

Photoreceptors absorptance spectra, $\propto_j (\lambda)$ = (j = L, M, or S) for L-, M- and S-cone photo-pigments are calculated using the following equations;

$$\propto_j (\lambda) = 1\text{-}10^{-D_{max.photopig.j} A_{shift.j}(\lambda)} \quad (7)$$

$$A_{shift.j}(\lambda) = A_j(\lambda - s_j) \quad (8)$$

$$D_{max.photopig,L} = (0.38 + 0.54e^{-v/1.333})(1+d_L/100)$$
$$D_{max.photopig,M} = (0.38 + 0.54e^{-v/1.333})(1+d_M/100) \quad (9)$$
$$D_{max.photopig,S} = (0.38 + 0.54e^{-v/1.333})(1+d_S/100)$$

where, $D_{max.photopig,j}$ denotes a specific cone type peak optical density, $A_{shift.j}(\lambda)$ shows a given cone type shifted low optical density spectral absorbance, and $A_j(\lambda)$ represents a specific cone type average low optical density spectral absorbance.

Cone fundamentals, in terms of quanta, would be attained through combination of the three constituents for each cone as follows;

$$\begin{aligned} l_q(\lambda) &= \propto_l (\lambda) 10^{-D_{macula}(\lambda) - D_{ocul}(\lambda)} \\ m_q(\lambda) &= \propto_m (\lambda) 10^{-D_{macula}(\lambda) - D_{ocul}(\lambda)} \\ s_q(\lambda) &= \propto_s (\lambda) 10^{-D_{macula}(\lambda) - D_{ocul}(\lambda)} \end{aligned} \tag{10}$$

Cone fundamentals, in terms of energy, on the other hand, would be obtained using the following equations;

$$\begin{aligned} l(\lambda) &= \lambda l_q(\lambda) \\ m(\lambda) &= \lambda m_q(\lambda) \\ s(\lambda) &= \lambda s_q(\lambda) \end{aligned} \tag{11}$$

Finally, the three obtained functions would be normalized so that each function maximum value would be unity. Therefore, Monte Carlo simulation was used, and different observers' CMFs could be simulated for different field sizes.

2.2. Spectral Reflectance Recovery from CIEXYZ

Because it is attempted to extend the main idea presented in this paper to the spectral recovery from CIEXYZ tristimulus values, some of the recent papers published in this area are touched upon in this section.

Different approaches have been devised for spectral recovery from CIEXYZ tristimulus values. Principal Component Analysis (PCA), Non-Negative Matrix Factorization (NNMF), Interpolation, Pseudo-Inverse and so on. Many papers have also strived to either amalgamate different approaches or enhance the original method through making some modifications.

Agahian et al. devised weighted PCA and applied that to spectral recovery process [11]. In an ordinary PCA, eigenvectors (or basis functions) of learning samples are extracted. Those eigenvectors are then used as primaries and the spectra of the testing samples are recovered using them. In the method proposed by Agahian et al., weights were first computed that were based on colorimetric difference between each testing sample and all the learning ones in a way that the bigger the difference, the smaller the influence of that particular learning sample on the extraction of the basis functions used in spectral recovery. In other words, the basis functions would change for each testing sample depending on how similar or different testing samples are as compared to the learning ones, colorimetrically. It was shown that this method could lead to a far better accuracy in comparison to classical PCA in which all the eigenvectors are extracted without considering how far the testing samples are from the learning ones.

Kim et al. came up with a hybrid method for spectral recovery [17]. They combined different methods together, namely, 3D interpolation, 2D interpolation, and adaptive NNMF. The 3D interpolation was applied using CIEXYZ tristimulus values. 2D interpolation, on the other hand, was performed using CIExyY values. Adaptive NNMF refers to the use of learning samples near the testing ones; in other words, not all the learning samples were used. In order to do that, they used goodness of fit as a criterion and

after applying the ordinary NNMF, they only chose learning samples leading to a better recovery for the testing ones. The logic behind amalgamating different approaches is observed when interpolation is applied, not all the testing samples get to be reconstructed from learning ones and some of the testing samples happen to fall out of the color gamut of learning samples. For those samples falling outside the learning samples' color gamut, adaptive NNMF was employed.

Amiri and Amirshahi devised a weighted regression and implemented it along with PCA and NNMF [23]; they stated that in the ordinary PCA, there is only the possibility of using three eigenvectors. This limitation comes from the fact that for testing samples only three CIEXYZ tristimulus values under a particular illuminant are accessible, while for learning samples, CIEXYZ under other light sources can be readily accessed. Thus, a matrix can be calculated relating the CIEXYZ under that specific illuminant to other sets of tristimulus values under other sources. Then, the same matrix is applied to testing samples to predict their tristimulus values under other light sources. Therefore, using regression they were able to predict CIEXYZ tristimulus values of testing samples under other light sources. They also come to the conclusion that the accuracy by which the tristimulus values of the testing samples are obtained is of great importance. Consequently, they came up with the weighted regression in which the tristimulus values of learning samples are multiplied by weighting factors based on the difference between tristimulus values of testing and learning samples; in other words, the larger the colorimetric difference between the testing and learning samples, the smaller the weight, and hence the smaller the influence of that specific learning sample on calculating the matrix of transform. Therefore, using weighted regression, they were able to accurately predict the tristimulus values of testing samples

under different light sources, and thus to use a larger number of eigenvectors in the recovery process leading to a more precise reconstructed spectral reflectance for testing samples.

Cao et al. improved Pseudo-Inverse method through imparting a weight matrix into the process [29]; the matrix of weight was calculated based on the both colorimetric and spectral similarities of the testing and training samples. In order for them to calculate the spectral similarities of the testing and training samples, they needed to first estimate the testing data spectra; therefore, they used a simple pseudo-inverse method to determine their spectra and used those reflectance spectra to calculate the spectral similarities of the testing and training samples. They showed, at the end, that applying the weight matrix to the simple pseudo-inverse method would improve the recovery accuracy in a significant manner.

2.3. Spectral Reflectance Recovery from RGB Camera Response

Methods used for spectral reconstruction from camera RGB responses have also attracted a great deal of attention; they are interesting in that they do not use a standardized color spaces such as CIEXYZ. Some of the most recent papers in this area is presented herein.

Valero et al. stated that using an RGB camera along with several colored filters could help recover the spectra accurately enough even for practical applications; in a simulation, they utilized an RGB digital camera along with 3 colored filters to take a photo of scenes that were obtained from a database of hyperspectral image. They used the camera without any filters, with 1 filter (each one of a set of 5), with 2 filters (4 different combinations of 2 filters) and finally with 3 filters (2 different amalgamations). Higher filter combinatins

were selected from the best performing lower filter combination. At the end, they observed that the larger the number of filters, the better the recovery accuracy. It is worth mentioning that they have used pseudo-inverse method for spectral recovery.

Zhao and Berns used a digital camera and modified it through utilization of a filter slider that held 2 custom-designed filters to capture two consecutive sets of RGB images generating 6 channel camera images [26]. They used one transform matrix (pseudo-inverse method) from camera response to spectral information and another one from camera response to colorimetric information under a specific viewing condition. They asserted that using a separate transform for each leads to a better results both spectrally and colorimetrically. At the end, they used matrix R method to associate the spectral reflectance they obtained with the colorimetric information as first detailed by Wyszecki.

Cao et al. devised a weighted method of spectral recovery in which spcectral reflectance of the testing samples were reconstructed using a few learning samples falling near them [30]. They stated that each testing spectral reflectance can be recovered through a weighted sum of a few learning samples falling beside the testing samples. In order for them to decide on the learning samples falling near the testing samples, they used color difference in CIELAB color space and chose thoese learning samples that possess the smallest color difference from the testing ones. They assume that the RGB camera response follows the sRGB standard formula, and they simply convert those RGB to CIELAB. This method, as one of the most recent methods in spectral reflectance recovery from RGB camera response is further explained and its results will be compared to several other methods that are devised in this thesis.

Cao et al. used also a sample selection method for the spectral recovery [31]; in this method, they made use of a criterion to only pick a few learning samples falling near the testing samples in terms of colorimetric difference. To clarify, they used a colorimetric difference value and placed that as a limit and only used learning samples inside this limit for determination of the matrix transform in the spectral recovery (pseudo-inverse method). In other words, each testing sample would have its own specific transform matrix calculated using a few neighboring learning samples.

2.4. Spectral Reflectance Recovery from Multi-Spectral Camera Response

In this work, multi-spectral imaging system is simulated through assuming that seven colored filters are placed in front of a monochrome sensor. In this section a few of the works published in the area of spectral imaging using multi-spectral cameras are presented. Shimano et al. assembled a multi-spectral camera with seven channels using seven interference filters along with a monochrome CCD camera [16]. In a comprehensive study, they used their system and took a picture of their targets. Afterwards, they utilized several different methods such as Wiener estimation, pseudo-inverse, and PCA, for recovering the spectra from the camera response. They compared the recovery accuracy and came to the conclusion that Wiener estimation leads to the most accurate results.

Shrestha et al. stated that even though the accuracy by which the spectral reflectance of a scene is obtained is very high in the case of the multi-spectral imaging cameras, the restriction imposed by the system, e.g., having to take several photos for each channel, and having to register the images for each channel would prevent the system from being used in daily applications [32]. Therefore, they came up with a new multi-spectral imaging

system capable of taking the image in only one shot. The system would use two RGB cameras with the same resolution in a stereoscopic configuration and a pair of suitable filters placed in front of each camera. The filters are selected in a way that they will modify the sensitivities of one or both cameras to produce 6 well-spaced channels across the visible spectrum. The amalgamation of the images from both cameras would generate a multi-spectral image of the scene. They asserted that one shot acquisition can be obtained using two cameras with a sync controller, which is accessible in market. Therefore, the system acts as a two-in-one multi-spectral-stereo system. The system they assembled, would not only capture the multi-spectral images through only one shot, but it is also capable of capturing 3D images.

3. Experiment and Procedure

This work is split into two main sections; the first section is concentrated on the humans' and cameras' spectral sensitivity variability theory with respect to spectral recovery. The second section of the thesis attends to real situations and is composed of 3 subsections. In the first section, results of the recovery using real cameras and smartphones are presented. The second and third sections describe 2 approaches, regression and color matching, respectively, to simulate observers' response; both of these approaches could be used in an authentic situations.

3.1. Theory

3.1.1. Human

It has been demonstrated that increase in a specific object's colorimetric information utilizing different approaches such as capturing colorimetric information under a diverse range of illuminations, utilization of colored filters in front of RGB cameras and so forth will enhance the recovery accuracy of the spectral information. Filters and light sources can be regarded as having similar impact on deriving different colorimetric datasets for a specific object. As we all know, an object color depends upon 3 different factors, light source under which the object is seen, the object reflectance and the observer seeing the object. This indicates that another way in order to increase the colorimetric information is to record different observers' colorimetric response to a colored object. At the first glance, this work might seem impossible, however, Asano et al. have devised a vision model simulating different observers' CMFs, which aids in the reflectance spectra recovery using those simulated CMFs. It should be noted though that CMFs generated by their model are

lms-CMFs; it means the CMFs is in the LMS space or in other words, they are cone fundamentals comprising lens and macular pigment transmittance and also the sensitivities of cone photoreceptors. However, using a linear transformation supplied by the authors, the CMFs were tranformed to xyz-like CMFs for a 10 degree visual field. To clarify, the CMFs are in a space similar to CIEXYZ. Thus, the aim is to demonstrate that if the colorimetric response of the observers can be attained, they can then be put into use in the spectral recovery process to enhance the accuracy. Given two spectral dataset denoted by **Rl** (whose size is sa×n, where n is the number of learning samples and sa is the number of sampling points and m is the number of testing samples) and **Rt** (whose size is sa×m, where m is the number of testing samples), they represent the learning and testing samples, respectively. To clarify, the **Rt** spectra are estimated using the model fit to **Rl** spectra. A specific light source spectral power distribution is denoted by **L**, and the CMFs attained from the Asano's model are shown by **CM** (whose size is 3no×sa, where no shows the number of observers). The **CM** matrix contains the CMFs of 20 observers. The following formulas are utilized to obtain the observers' colorimetric response.

$$\mathbf{Cl}=k\times\mathbf{CM}\times\mathrm{diag}(\mathbf{L})\times\mathbf{Rl} \quad (12)$$

$$\mathbf{Ct}=k\times\mathbf{CM}\times\mathrm{diag}(\mathbf{L})\times\mathbf{Rt} \quad (13)$$

where, k is a normalizing factors such that the perfect reflecting diffuser Y would be 100 and it also depends on the particular observer, diag denotes the diagonal matrix of the light source spectral power distribution utilized in the formula and **Cl** and **Ct** are the two matrices that contain the XYZ_n (subscript n is utilized since they are not precisely CIEXYZ tristimulus values, but the simulated ones using Asano's model) of the learning and testing

samples given by the observers possessing their own specific CMFs. First, the learning set is used to specify the relationship of the spectral and colorimetric data through utilization of simple pseudo-inverse approach shown as follows:

$$\mathbf{M}=\mathbf{Rl}\times pinv(\mathbf{Cl}) \quad (14)$$

where, *pinv* shows the pseudo-inverse and matrix **M** contains the relationship between the reflectance spectra and XYZ_n colorimetric data. This matrix is then multiplied by the testing samples' XYZ_n to reconstruct their reflectance spectra as follows:

$$\mathbf{Rr}=\mathbf{M}\times\mathbf{Ct} \quad (15)$$

where, **Rr** denotes the testing samples' reconstructed reflectance spectra. The purpose of this section is to show that the larger the number of colorimetric individuals' response, the more accurate the recovery will be. The X, Y and Z that each observer would give using the Asano's model are being simulated and then put into the reflectance spectra recovery attempt to see the impact of increase in the number of observers.

3.1.2. Camera

Cameras bear a close resemblance to human vision in normally possessing 3 color channels (usually denoted by R, G and B standing for Red, Green and Blue, respectively), each of which has its own specific spectral sensitivity that correspond to long, middle and short wavelength light; moreover, there is a variability among different cameras' spectral sensitivity functions that is similar to humans', which could be utilized to more accurately recover the spectra through amalgamating different cameras' RGB responses, as done in the above section in the case of the humans. Different cameras' spectral sensitivity functions are attained from an open database [33]. Figure 1 illustrates the sensitivity functions of 13 different types of cameras, namely, Canon 1D Mark III, Canon 20D, Canon

300D, Canon 40D, Canon 500D, Canon 50D, Canon 5D Mark II, Canon 600D, Canon 60D, Hasselblad H2, Nikon D3X, Nikon D200 and Nikon D3 that are used in this work.

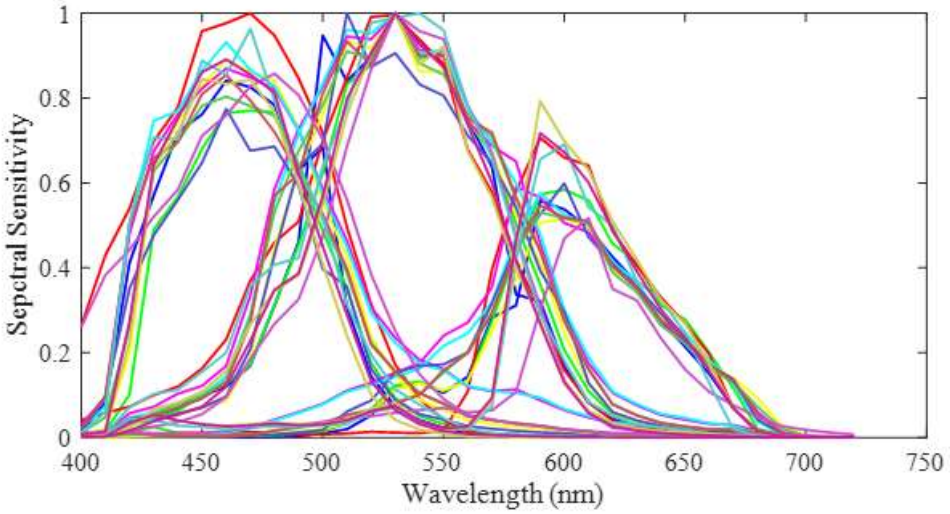

Figure 1, Spectral sensitivity of different types of cameras used in this work.

These cameras' responses to the testing and learning targets are acquired through simulation and using the approach describedin the former section, the reflectance spectra of the testing samples are recovered from the learning ones. The cameras' response to the learning and testing samples are captured using similar equations to 12 and 13 in the preceding section; however rather than matrix **CM**, sensitivities of the cameras are utilized

3.2. Practice

3.2.1. Real Cameras

In this section, results of the spectral recovery using different types of real smartphones and cameras are presented to test the mean idea in this work, which is the larger the number of cameras used in the spectral recovery process, the better the recovery accuracy will be. This part is indeed the section 3.1.2 authentic version, in which real cameras are put into use for spectral reflectance recovery process. 6 smartphones, namely, Nokia Lumia 635, Samsung Galaxy s6, iPhone 7, LG Nexus 5, iPhone 6s, and iPhone 6 and four cameras,

namely, Nikon D2H, Nikon D40, Nikon D60, and Canon 60D were used. Testing and learning targets' pictures were taken in the light booth under 3 different light sources. The mean patch values of the testing and learning samples are used as camera response; then equation 14 was used to obtain the matrix **M** between the spectra of the learning samples and the mean patch values of the same set. It should be noted that instead of **CI**, colorimetic reposne of the observer, RGB camera response is used in equation 14. Afterwards, equation 15 is utilized to obtain the spectra of the testing samples from the camera response of the same set. It should be noted that each camera is used under 3 different light sources, A, Tl84 and D64, and three different pictures are taken of the targets. Then, using the learning samples, only pictures that would result in a better spectral recovery was used. The results for cameras and smartphones are reported separately.

Moreover, as mentioned in the literature review section, Cao et al.'s method, as one of the most recent approach to spectral recovery from camera response is compared with several other newly devised methods in this thesis.

The recovered spectra do not have a high colorimetric accuracy compared to their original ones and thus it is found out that taking separate paths, one for spectral and one for colorimetric recovery would lead to a better result, which is explained as follows. The workflow proposed herein can be used whenever ordinary cameras and smartphones are used in an attempt to recover the spectra and also to simulate the color of an object under a diverse range of illumination types. In other words, the spectral path can be used for the spectral recovery at an acceptable level of spectral accuracy and the colorimetric path could be used for more accurate visualization of the object under different lighting and viewing conditions.

3.2.1.1. Spectral Path

For the spectral path, different smartphones' and cameras' responses were combined to see the effect of the increase in the number of cameras on the spectral recovery accuracy. Two different methods were applied; in the first method, different camera response would be combined in a random fashion but in the second approach a technique called stepwise selection of cameras, in which cameras are combined according to how accurate they are in spectral recovery is applied. In other words, in the second approach, first the best camera is selected, then the second best camera is added to the process which would lead to the best recovery. Even though this would help reconstruct the spectra better, this method is of little value in real situation where there is no access to the spectra of the samples to check which cellphone or camera to use. Generally, the more different the cameras' spectral sensitivity from each other, the more accurate the recovered reflectance is when their responses are added together. This path could help identify the material being imaged even though the colorimetric accuracy is not very high. Also, some algorithm of color matching such as Allen, used extensively in Textile industry, needs the spectral reflectance of the sample being matched as an input, which can be estimated using the method proposed herein. In other words, for the aim of identification and color matching, this path could help in a significant manner, however, since the colorimetric accuracy of the finally recovered spectral reflectance is not so high, it is better to take a separate path for the colorimetric characterization of the object explained as follows.

3.2.1.2. Comparison

In this section, Cao et al.'s method [4] along with 4 devised methods are briefly explained and their results are compared to each other in this section. In their work, they only used one camera.

Let us first explain the approach suggested by Cao et al..

They came up with a technique for recosntructing the spectral reflectance of the objects photographed by an RGB digital camera; first, they transformed the RGB camera response to CIELAB for both testing and learning samples. After that, they computed the color difference between the testing specimens and all the learning ones utilizing the following formula.

$$\Delta E_{a*b*} = \sqrt{(L^*_{train} - L^*_{test})^2 + (a^*_{train} - a^*_{test})^2 + (b^*_{train} - b^*_{test})^2} \qquad (16)$$

where, L*, a*, and b* with test subscripts refer to the testing samples' coordinates, and L*, a* and b* having train subscripts refer to the training samples coordinates.

Afterwards, they devised 4 formulae to estimate the spectral reflectances of the testing samples, however, according to authors themselves, the first one results in the best result, thus the same formula is also used herein, which is further explained as follows. They asserted that the spectral reflectance of the testing samples could be estimated through a weighted average of samples' reflectance in a selected training group of specimens; they set a criterion for opting for the group of samples from training samples, which is the equation 16. In other words, n training specimens that have a smaller color difference from the testing ones were used for reconstructing the reflectance spectra of the testing samples through utilization of the following formula.

$$R_{est} = k\times(R_1/\Delta E_1^2 + R_2/\Delta E_2^2 \ \ldots \ Rn/\Delta E_n^2)$$
$$k = 1/(1/\Delta E_1^2 + 1/\Delta E_2^2 \ \ldots \ 1/\Delta E_n^2) \quad (17)$$

where, $\Delta E_1, \ldots, \Delta E_n$ are the n color difference calculated using the intended testing sample and the learning ones, and $R_1, \ldots R_n$ are the n learning samples' spectra, and R_{est} is the estimated spectral reflectance of the intended testing sample. n samples are in fact the group of learning samples falling near the testing one in terms of color difference. They stated that the number of training samples around the intended testing sample is not a matter of great importance. Consequently, in this work, 15 training samples around each testing sample is selected (as used by the authors as well). To better compare their work to the work proposed herein, some points are raised. First, they used sRGB formula to transform the RGB response of the camera directly to CIELAB assuming that the RGB response of the camera follows sRGB standard formula. Thus, the same thing is applied in this work, to show that even though their method has simplified the procedure greatly exempting one from endeavoring to come up with formula to estimate CIEXYZ from camera response, it would not evidently work for the majority of the commonly utilized RGB cameras in which it is not determined what formula exactly the cameras follow when it comes to transform from RGB to CIEXYZ values.

Therefore, in the first approach suggested this work, the nonstandard RGB space of the camera itself is used, even though it is a nonstandard space, it contains at least all the information that the RGB camera has captured. It is of fundamental importance to linearize the camera photometric response (that is explained in the colorimetric path section of Experiment and Procedure) so that they could be linearly associated with Y tristimulus value. Thus, the proposed approach by Cao et al. is a bit modified in a manner that rather

than computing the color difference using the CIELAB values of the testing and training samples, it is calculated from linearized RGB camera response directly as shown in equation 21. Everything else is similar to the paper published by Cao et al., however, the formula for color difference using which learning samples around a testing one are selected does not make use of CIELAB. Simply put, training samples near the testing samples are chosen on the basis of RGB camera response.

The second method that is proposed herein for spectral recovery is weighted pseudo-inverse. Since pseudo-inverse is a method often used for spectral recovery, it is then enhanced through incorporating a weighting function into it. The weights are computed using the same formula as 29 on the basis of the Euclidean distance between the linearized RGB camera response to the learning and testing samples as in equation 21. After putting the weights for each testing sample in diagonal matrix as in equation 30, the weights would be then imparted to equation 14 as follows to calculate the matrix **Mn** between the spectral and RGB information of learning samples.

$$\mathbf{Mn}=\mathbf{REFl}\times\mathbf{W}\times pinv(\mathbf{RGBl}\times\mathbf{W}) \quad (18)$$

Therefore, matrix **Mn** would be different depending on the particular testing sample. Multiplying matrix **Mn** by the linearized RGB camera response results in their estimated reflectance spectra.

It would also be worthwhile to make use of nonlinear regression and also nonlinear weighted regression for spectral recovery to compare their results to the above mentioned methdos. In order to use nonlinear regression, first RGB linearized camera response should be multiplied by each other to create a polynomial out of them. After multiplying the RGB terms together, they are used in the following equation.

Mnr= **REFl** ×*pinv*(**RGBlin_Ln**) (19)

RGBlin_Ln =

$$[1 \quad R \quad G \quad B \quad RG \quad RB \quad GB \quad R^2 \quad G^2 \quad B^2 \quad RGB \quad R^2G \quad G^2B \quad B^2R \quad R^2B \quad G^2R \quad B^2G]^T$$

(20)

where, **RGBlin_Ln** is the matrix that also contains the multiplication terms of RGB for learning samples and **Mnr** is the matrix containing the relationship between the spectral and RGB information of learning samples. Therefore, by multiplying the matrix **Mnr** by the matrix containing the RGB camera response of testing samples that also contains their multiplications the same as **RGBlin_Ln,** it is possible to obtain their spectral reflectance. The nonlinear regression used is a polynomial with 17 coefficients that reportedly leads to a satisfactory result [3]. Weighted nonlinear regression is also made use of which is the same as nonlinear regression but it also weights the training specimens according to how far apart they are from the testing ones. The farther the training specimens from the testing ones, the lower the weight that they receive. The weighted nonlinear regression is the similar to the weighted pseudo-inverse, nonetheless, it is only nonlinear regression. Nonlinear regression and its weighted version is further explained in section 3.2.2.

Therefore, there are seven different approaches here to compare with each other; first is the random addition of cameras, second is the same as the first one but for smartphones, third is the stepwise addition of cameras, fourth is the same as the third one but for smartphones, fifth is the method proposed by Cao et al., sixth is modified version of the Cao et al.'s method where the RGB camera response are directly utilized for calculating the distance between the learning and testing samples, seventh is weighted pseudo-inverse, eighth is the nonlinear regression and ninth is the weighted nonlinear regression that are referred to as

ran-ph, ran-cam, step-ph, step-cam, Cao, Cao mod, wt-pinv, nonlin, wt-nonlin, respectively, from here on. The best camera in terms of colorimetric accuracy is specified in the colorimetric path, the same camera is also used for making a comparison between these seven approaches as well.

3.2.1.3. Colorimetric Path

As mentioned above, it is found out that putting together different cameras' responses to recover the spectra did not lead to an accurate colorimetric characterization of the camera. In order to better characterize a color of the object under a specific lighting and viewing condition, a separate path, named colorimetric path is taken. 3 different stages are taken in this path explained as follows; first, the best camera, from among the smartphones and cameras was picked which would lead to a better colorimetric characterization of the object than other cameras. Second, the most suitable distance at which the colorimetric characterization is the most accurate is found for that specific camera. Third, after choosing the best camera and the most suitable distance at which the camera can work the best, different kinds of linear and nonlinear transforms from camera response to colorimetric values under a specific viewing condition are utilized. The colorimetric values belong to a specific standard observer and viewing condition. Therefore, the simplest method for transforming the camera response to this colorimetric set is to use equation 14 and find a matrix relating the camera response to a specific set of colorimetric information. Equation 19 is another viable option that would be used as a nonlinear regression model. The weighted regression is also used along with the nonlinear regression to compare its results to other methods. Using weighted regression, each testing sample would possess its own specific transform matrix. The weights are computed based on the distance between the

linearized RGB camera response of testing and learning samples. Four different formulae for calculating the distance are used herein to see which one leads to a better accuracy.

The first formula is on the basis of Euclidean distance as in 3.2.2, shown as follows:

$$\Delta E_{Eu}= \sqrt{(Rlin\_T - Rlin\_L)^2 + (Glin\_T - Glin\_L)^2 + (Blin\_T - Blin\_L)^2} \quad (21)$$

where, ΔE_{Eu} is Euclidean distance, Rlin_L, Glin_L and Blin_L are linearized camera response to learning samples and Rlin_T, Glin_T and Blin_T are the linearized RGB camera response to testing samples. The formula is referred to as formula 1.

The next formula for calculating distance is Minkowski distance, given as follows:

$$\Delta E_{Mi}= \sqrt[p]{(Rlin\_T - Rlin\_L)^p + (Glin\_T - Glin\_L)^p + (Blin\_T - Blin\_L)^p} \quad (22)$$

where, ΔE_{Mi} is the Minkowski distance; using learning samples, it is found out that p=0.5 works better; the formula is referred to as formula 2.

The third formula is called city block, shown as follows:

$$\Delta E_{CB} = |Rlin\_T - Rlin\_L| + |Glin\_T - Glin\_L| + |Blin\_T - Blin\_L| \quad (23)$$

where, ΔE_{CB} is the Minkowski distance; this formula is referred to as formula 3.

The last formula named is Chebyshev distance, demonstrated as follows.

$$\Delta E_{Ch} = \mathrm{Max_j}\{|RGBlin\_T_{m\times 3} - RGBlin\_L_{n\times 3}|\} \quad (24)$$

where, ΔE_{Ch} is the Chebyshev distance; this formula is referred to as formula 4.

Now that the distance has been computed, weights are then calculated as follows:

$$W_i=\frac{1}{\Delta Ei+s} \quad (25)$$

In order to prevent the weights from becoming infinity in case ΔE (one of the formula 1, 2, 3 or 4 for calculating the distance) is zero, s which is equal to 0.01 is used. The distance is calculated between each testing sample and the whole learning set. Therefore, there are

n different weights for each testing sample; now that the weights are computed, they are placed in a diagonal matrix as shown in the following manner for each testing sample.

$$\mathbf{W} = \begin{bmatrix} W_1 & 0 & \cdots & 0 & 0 \\ 0 & W_2 & & 0 & 0 \\ \vdots & & \ddots & \vdots & \\ 0 & 0 & & W_{n-1} & 0 \\ 0 & 0 & \cdots & 0 & W_n \end{bmatrix} \quad (26)$$

After that, this n×n weighting matrix is used as follows:

$$\mathbf{Mn}=\mathbf{XYZl}\times\mathbf{W}\times pinv(\mathbf{RGBlin\_Ln}\times\mathbf{W}) \quad (27)$$

Where **XYZl** represents the XYZ of the learning samples; the **Mn** transform matrix is then multiplied by the linearized RGB of the testing samples to predict their CIEXYZ; it should be noted that using weighted regression, each testing sample possess its own specific matrix of transform.

Drawing upon optimization, in which the matrix **M** in equation 14 that relates the RGB camera response to CIEXYZ values, is optimized for the learning samples is yet another model that would be used in this work. The optimization used is fminsearch, which is an optimization algorithm commonly used in Matlab. Fminsearch is an unconstrained optimization with a nonlinear nature striving to locate the minmum of a scalar function of several variables. In order for this function to be able to start the optimization process, it is in need of an initial estimate, which is the matrix of trnaform obtained from a simple psudo-inverse. The advantage and disadvantage of each of the transforms were compared and the best one in terms of how fast and accurate the transform is chosen. At the end, some visualization was developed to show the colorimetric accuracy of the best transform. It should be noted that the camera photometric response is first linearized using neutral samples of the learning target [34]. In order to do that, the luminance factor of the neutral samples of the learning targets are linearized with respect to the normalized digital counts

(digital counts divided by 255, since the images are 8 bits per channel herein). Afterwards, different transform equations are applied to the linearized camera response to choose the most efficient one. The value of this section is in the visualization that these methods enable, which shows the object under different viewing conditions with an acceptable level of colorimetric accuracy.

3.2.2. Semi-real Human (Regression)

In this section, it is attempted to extend the idea given in this thesis to a series of ongoing research where spectra are estimated from their corresponding CIEXYZ tristimulus values. In this research, an assumption is made up front that in the case of the learning samples, the spectra are available, and therefore their tristimulus values under any viewing circumstances can be specified. However, in the case of the testing specimens, only the CIEXYZ tristimulus values under a particular condition is known. It should be noted that the CIEXYZ used in this research belongs to one of the CIE standard observers, either 1931 or 1964 (CIE 1964 standard observer is selected herein). Consequently, for this section, one set of standard observer's CMFs are accessible in conjunction with other observers' CMFs simulated using Asano's model. The matrix containing the standard observer's CMFs is shown by **SC**, and the matrix containing other simulated observers' CMFs is denoted by **OC**. Now, using each CMFs set available, a separate XYZ (**XYZs** for the standard observer and **XYZo** for the simulated ones) is obtained for the learning specimens shown as follows.

$$\mathbf{XYZs} = k \times \mathbf{SC} \times \mathrm{diag}(\mathbf{L}) \times \mathbf{Rl} \qquad (28)$$

$$\mathbf{XYZo} = k \times \mathbf{OC} \times \mathrm{diag}(\mathbf{L}) \times \mathbf{Rt} \quad (29)$$

where, k is a normalizing factor. Then, the two sets of XYZ are combined together in a single larger matrix as follows:

$$\mathbf{XYZa} = \begin{bmatrix} \mathbf{XYZs} \\ \mathbf{XYZo} \end{bmatrix} \quad (30)$$

Now, equation (14) is utilized and the matrix **M** between the learning samples' spectra and the **XYZa** of the same sample is acquired. Afterwards, matrix M is multiplied by the **XYZa** of the testing specimens. In the case of the testing samples, only XYZ of the standard observer is in hand, making the matrix **M** obtained from the learning specimens inapplicable to the testing ones utilizing similar methods as equations (28) and (29) is not feasible. Previous paper had almost the same issue, in which they intended to estimate the tristimulus values of the testing samples under different illumination conditions [23]. They suggested using weighted nonlinear regression and they found out that the best nonlinear regression for this aim is nonlinear polynomial with seventeen coefficients. In that paper, they had access to learning samples' CIEXYZ tristimulus values under illuminants A and D65, however, for the testing samples, they only had access to the tristimulus values under D65 standard illuminant. In order for them to acquire the tristimulus values under illuminant A for the testing specimens, they had to first find out the relationship between learning samples' XYZ under illuminant D65 and A and then apply it to the testing samples. They used different samples for testing (900 textile samples representing samples of Munsell color book and 1977 textile specimens) and learning (1269 Munsell chips samples from Munsell color book). Therefore, through utilization of all these specimens

and trying different linear and nonlinear regression types, they concluded that nonlinear polynomial with 17 coefficients performed in a satisfactory manner for both testing and learning samples. A similar method is used herein; to clarify, using the relationship between the standard observer's XYZ and the simulated ones' in the case of the learning samples, the XYZ of the simulated observers in the case of the testing samples, are estimated. The regression equation is given as follows:

$$\begin{bmatrix} X \\ Y \\ Z \end{bmatrix}_{o} = \begin{bmatrix} a_{1,1} & a_{1,2} & \dots & a_{1,17} \\ a_{2,1} & a_{2,2} & \dots & a_{2,17} \\ a_{3,1} & a_{3,2} & & a_{3,17} \end{bmatrix} \times [1 \quad X \quad Y \quad Z \quad XY \quad XZ \quad YZ \quad X^2 \quad Y^2 \quad Z^2 \quad XYZ \quad X^2Y \quad Y^2Z \quad Z^2X \quad X^2Z \quad Y^2X \quad Z^2Y]_{s}^{T} \tag{31}$$

where, subscripts s and o denote the learning samples' XYZ of standard and other simulated observers, respectively. Afterwards, the same transform matrix is applied to the testing specimens in order to estimate the response of the simulated observers to the testing specimens. On the other hand, weighted regression has the privilege of calculating a separate matrix of transform for each testing specimen. The weights are computed on the basis of the Euclidean distance in CIELAB color space between the testing and the learning specimens utilizing standard observer's color specifications denoted by ΔE

$$W_i = \frac{1}{\Delta E_i + s} \tag{32}$$

where, s is 0.01 preventing from infinity when ΔE is zero. Euclidean distance between each testing specimen and all the learning samples are calculated. there will be n different weights for each testing samples if there are n learning specimens; after calculating the

weights, they are arranged in the following way in a diagonal matrix for each testing specimen.

$$\mathbf{W} = \begin{bmatrix} W_1 & 0 & \cdots & 0 & 0 \\ 0 & W_2 & & 0 & 0 \\ \vdots & & \ddots & \vdots & \\ 0 & 0 & & W_{n-1} & 0 \\ 0 & 0 & \cdots & 0 & W_n \end{bmatrix} \quad (33)$$

Afterwards, this n × n matrix of weights is multiplied by equation (31) as follows:

$$\mathbf{Tr} = \mathbf{XYZo} \times \mathbf{W} \times pinv(\mathbf{XYZse} \times \mathbf{W}) \quad (34)$$

where, **XYZo** shows the simulated observers XYZ and **XYZse** denotes the standard observer's XYZ (, which also contains multiplication of the terms X, Y and Z by each other, as in equation 8) for the learning specimens. Matrix **XYZse** should not be mixed up with **XYZs** in equation 28, since it also comprises terms multiplication. Subsequent to attaining the matrix of transform (Tr), it is then multiplied by the testing samples' XYZ of the standard observer resulting in the estimated response of the simulated observers to the testing specimens. Thus, each testing sample would possess its own particular matrix of transform making the simulated observer's estimated response more precise. Readers who are interested are referred to the paper [23] for more information on the weighted regression technique.

Both weighted and non-weighted regressions are used and the results are compared to specify which would result in a better recovery. After specification of the matrix of transform, it is applied to the testing specimens in order to estimate the XYZ of the simulated observers from those of the standard observer's. Now, **XYZa** can be formed for the testing specimens utilizing the XYZ of the standard observer (which was already

available) and the simulated observers' XYZ (which is estimated utilizing the weighted and non-weighted regression). As a result, matrix **M** which contains the relationship between the learning samples' **XYZa** and their spectra can be applied to the testing samples' **XYZa** in order to reconstruct their spectra. Using this approach, one can take advantage of increasing the number of observers in the recovery process; the idea is to again see if the same trend of recovery accuracy would be observed in this section as the ones in the prior sections, when the number of observers increases.

3.2.3. Semi-real Human (Color Matching)

In this section of the thesis, another method for obtaining the colorimetric response of the observers is described. This approach is the same as the approach detailed by Asano et al. [9]. It should be noted that in this work, the response of the observers is simulated that can be performed either though the approach suggested in 3.1.1 or in 3.2.2 or the method described herein which is called color matching.

For a given color match, there are a reference spectrum that is called $\boldsymbol{Sp_{ref}}$whose size is sa×1, where sa is the sampling point number across the visible spectrum, and three matching spectra of primaries that are called $\boldsymbol{Sp_{match,max}}$whose size is sa×3. In this work, the primaries are 3 Gaussian functions imitating 3 R, G and B –like primaries through which observers match the spectrum of the reference, as shown in Fig.2. The peak energy of the primaries are located at 440, 540 and 603 nm for blue, green and red primaries, respectively.

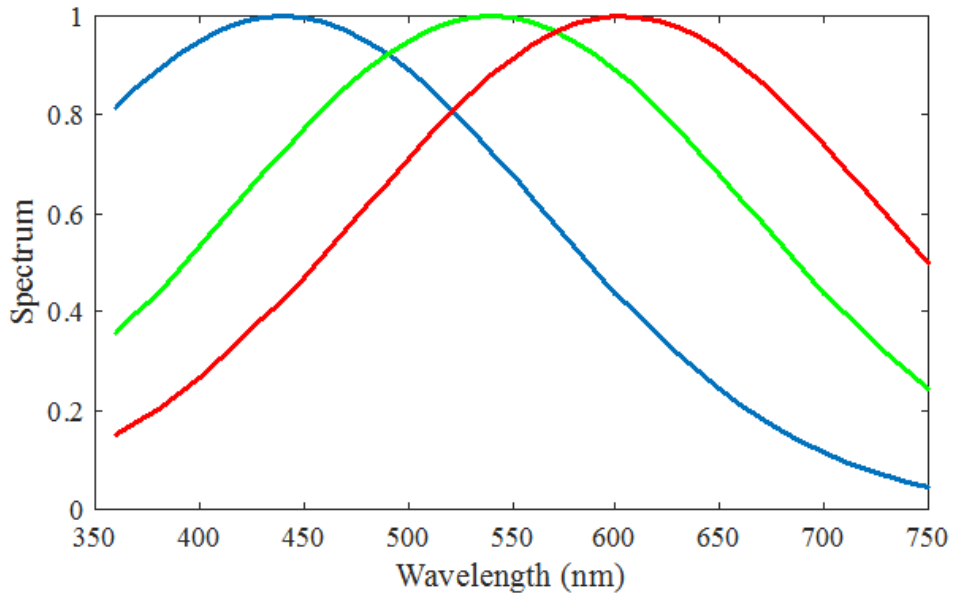

Figure 2. Gaussian primaries used for color matching.

Thus, a color match can be simulated for a specific observer with their own particular CMFs shown by $\boldsymbol{C_k}$ whose size is 3×sa. When a color match is attained between the reference and primary stimuli for a particular observer, the following equation holds.

$$\boldsymbol{C_k} \times \boldsymbol{Sp_{ref}} = \boldsymbol{C_k} \times \boldsymbol{Sp_{match,max}} \times \mathbf{R} \qquad (35)$$

Where, **R,** which is a vector of the size 3×1, contains scalars that modify the intensities of the three primaries to match the reference spectrum. **R** can be estimated using matrix inversion that is shown as follows.

$$\mathbf{R} = (\boldsymbol{C_k} \times \boldsymbol{Sp_{match,max}})^{-1} \times \boldsymbol{C_k} \times \boldsymbol{Sp_{ref}} \qquad (36)$$

The matched spectrum can then be recovered through the estimated scalars that are shown as follows:

$$\boldsymbol{Sp_{matched}} = \boldsymbol{Sp_{match,max}} \times \mathbf{R} \qquad (37)$$

Consequently, the matched spectrum can be changed to color utilizing the standard observer's spectral sensitivity functions under a specific viewing condition and it is then

made use of as the simulated observers' colorimetric response. Therefore, the similar observers that are simulated using the approach suggested by Asano et al. are utilized and their colorimetric response to both testing and learning specimens are obtained using the approach proposed herein. After that, through equation 14, matrix **M** between the reflectance spectra of the learning samples and the colorimetric response of the same set of samples is acquired; then, the same matrix is multiplied by the testing samples' colorimetric response (the same equation 15) in order to recover their reflectance spectra. In the real situations, there would not be a colorimetric response without any noise; therefore, in order to make the situation more realistic, random noise is also added to the response given by the observers using this approach. The random noise added follows a Gaussian model with a standard deviation of 1; the results when there is no noise and when there is random noise are compared to each other to find out the difference between them.

3.4. Multi-Spectral Imaging Camera

The main aim of the thesis is to examine the impact of the increase in the number of observers and/or cameras in the process of spectral recovery, which is done first using theoretical considerations and second using practice. At the end of the thesis, a comparison is drawn between the approaches suggested in this thesis and multi-spectral imaging and it is demonstrated that there is a great potential in the methods suggested herein that lead to the spectral recovery almost the same as that of the multi-spectral cameras. The multi-spectral imaging camera, in this work, is simulated using 7 different spectral transmittance of different filters which are illustrated in Fig.3. The multi-spectral camera is simulated in a manner that the filters are supposed to be placed in front of a monochrome sensor to take

seven photos of the stimuli. The response of the camera to the learning specimen is then utilized in equation (14) and matrix **M** which contains the relationship between the camera response and learning samples' reflectance spectra is obtained. Afterwards, the matrix is multiplied by the testing samples' response obtained from the camera to estimate their reflectance spectra.

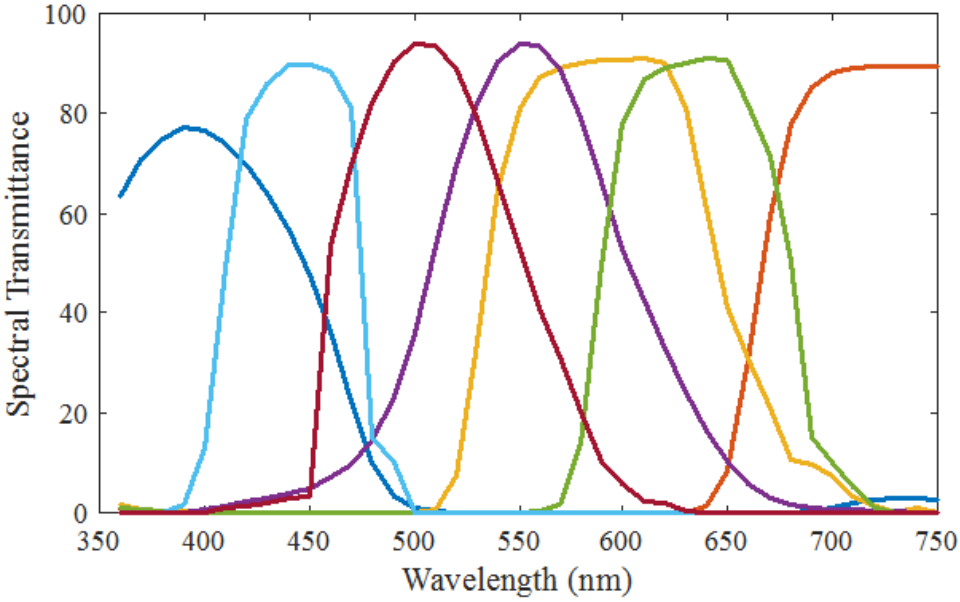

Figure 3. Filters used for the multi-spectral camera.

3.5. Datasets

3 datasets were used in the entire work; one as learning target and the other two as testing. 140 patch Macbeth ColorChecker was utilized as learning and 24 patch Macbeth ColorChecker, and 130 sample target made from Artist's paints were used as testing targets. The samples are shown in Fig.4. The 24 patch Macbeth ColorChecker is referred to as testing sample 1, and 130 sample target made from Artist's paint is referred to as testing sample 2 from here on.

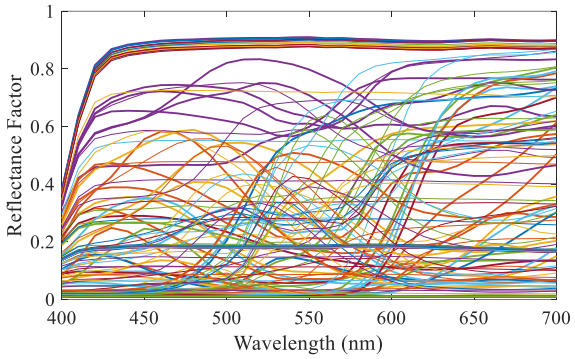

(1)

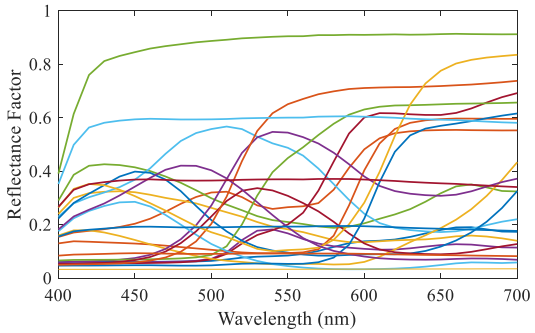

(2)

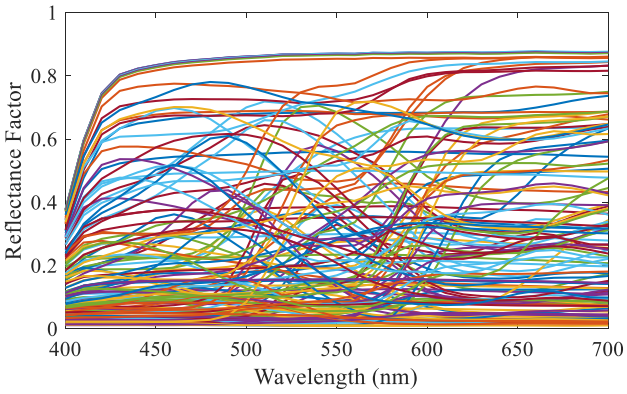

(3)

Figure 4. (1): learning and (2) and (3): testing samples1 and 2 used in this work.

Root mean squared error (*RMSE*) between the recovered and original reflectance spectra (that are reflectance factor with zero-to-one scale) and also color difference utilizing CIEDE2000 under a particular viewing condition are made use of as criteria to measure the accuracy of the spectral recovery process as the number of observers increases. Also, some of the spectral reflectance curves along with their recovered ones are presented to better show the precision of the proposed methods. Additionally, to better compare different colorimetric transform used for transforming the raw image taken by the camera to CIEXYZ tristimulus values under a specific viewing condition, some visualizations are made that are the output of each of the transforms used.

It should be noted that RMSE itself is not reported directly and it is however altered to $Log(100\times RMSE+1)$ to make the changes in the spectral error of recovery more correlated with the perceptual metric and also easier to compare; in other words, before taking the logarithm, *RMSE* is multiplied by 100 and 1 is added to the outcome of the multiplication because it is a fraction between 0 and 1, which makes logarithm, infinity in case *RMSE* is 0 and is negative when *RMSE* is a fraction. Thus, it was desirable to maintain results positive through making *RMSE* undergo a transform prior to taking the logarithm. The *RMSE* transformed version is referred to as spectral error from here on.

4. Results and Discussions

This section is split into two main parts each comprising several subsection corresponding to the subsections of the Experiment and Procedure section.

4.1. Theory

4.1.1. Human

In this part of the thesis, it is presumed that the observers' response to a specific colored specimen can be attained. In order to do that, Asano's model of color vision is used and 20 observers' CMFs are simulated, as shown in Fig.5.

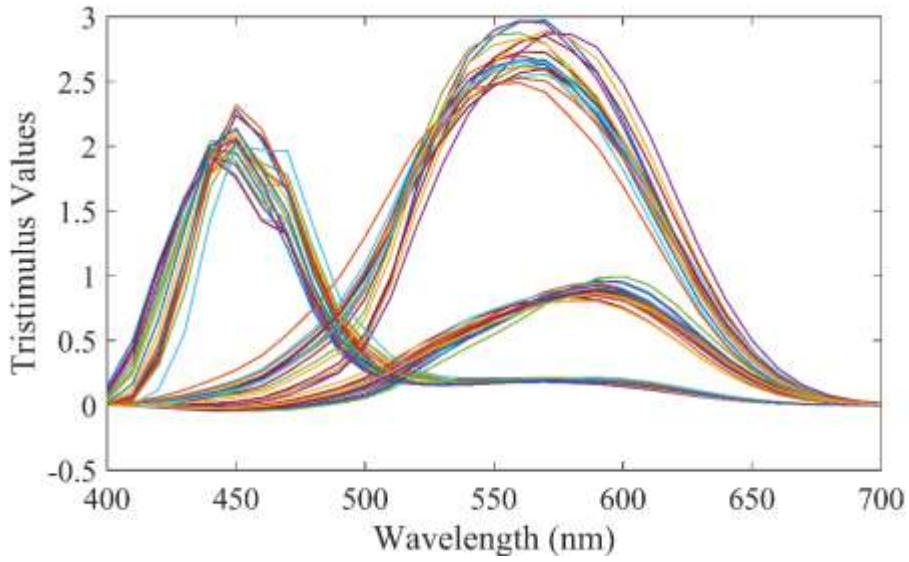

Figure 5. xyz-like CMFs of 20 simulated observers used in this work.

The next stage would be to amalgamate all these observers' response and use them to see how the accuracy of the spectral reflectance recovery alters as they are randomly added to the recovery process. To clarify, these observers' colorimetric responses to a given colored specimen is recorded or simulated herein, and utilized in the process of recovery of the

spectral reflectance. The mean spectral error trend between the original and the recovered spectral reflectances for the two testing samples are shown in Fig.6; as it is observed, increasing the number of observers substantially reduces the recovery error.

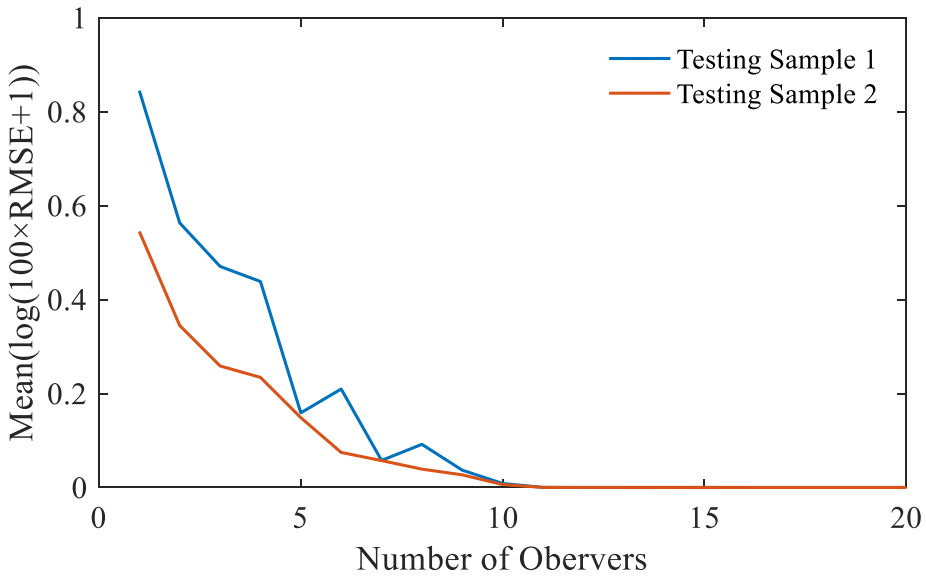

Figure 6. Trend of mean spectral error between the original and recovered reflectance spectra as the number of observers increases for the two testing samples.

The spectrum as a whole is integrated using three photoreceptors; people's visual capability is different, therefore, each would capture a particular part of the spectrum. They capture the spectrum and see it in their own specific 3 dimensional world. The spectrum itself can be thought of as a puzzle and each of us would hold a piece of this puzzle; if it is aimed to solve the puzzle, the pieces held by everyone are needed. As it is observed from Fig. 6, subsequent to adding about 10 observers, the spectral recovery error is drastically reduced to a point where it is basically zero. The error of zero here implies that there are ten observers capturing particular parts of the spectrum and when those parts are put together, the original spectrum has been obtained precisely. Also, as it is observed from Fig.6, even though the testing sample 1 possess a mean error that is bigger than the testing sample

(which is more easily observed when the number of observers are small), they both follow the same trend of results, meaning that after the addition of 10 observers to the process the error is basically zero.

It goes without saying that, combining the colorimetric response of people of different color vision would aid in reaching the spectrum itself more precisely.

Mean color difference under standard illuminant A between the original and the recovered spectra is also illustrated in Fig.7, the same way as in Fig.6. Since the observers' response were simulated using illuminant D65, it would be engrossing to calculate the color difference under other light sources than D65 itself.

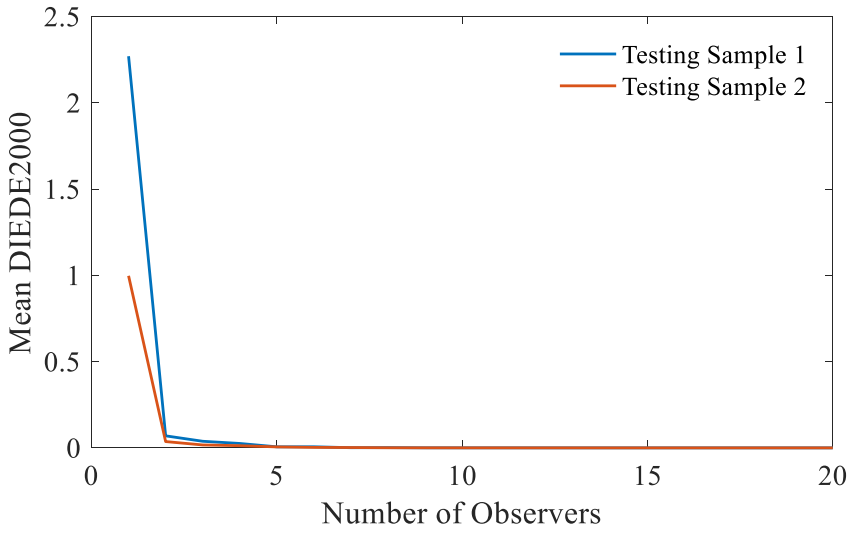

Figure 7. Trend of mean color difference as the number of observers increases in the recovery process under illuminant A.

Approximately, the same trend of results is observed in the mean color difference when the number of observers increases as in the mean spectral error. Nonetheless, the error in the colorimetric case has reached zero utilizing a smaller number of observers than in the case of Fig.6. It is no surprise observing such a difference in these two figures considering that Fig.6 illustrates the spectral error, however, Fig.7 reports the colorimetric error of the

recovery. To clarify, in Fig.7, the spectral sensitivity functions of the standard observer (1964 herein) has been employed to reduce the whole spectrum to only three colorimetric values throwing away some of the data at other parts of the spectrum where standard observer possesses no sensitivity. On the other hand, the spectral error shown in Fig.6 illustrates the difference between two spectral reflectances with a large number of sampling points across the spectrum. Therefore, it is not anticipated these two error to act the same as each other. Indeed, in the literature, use of both error is recommended [14, 23, 34]. At the end of this part, it would be worthwhile to show 4 randomly selected spectra along with their recovered ones for 1, 3, 5, 10 and 15 observers for each testing sample separately. Figs. 8 and 9 show the original and the recovered ones. Because the error of the recovery is very low in the case of 15 and 20 observers, they look similar that the result concerning 20 observers was excluded from here.

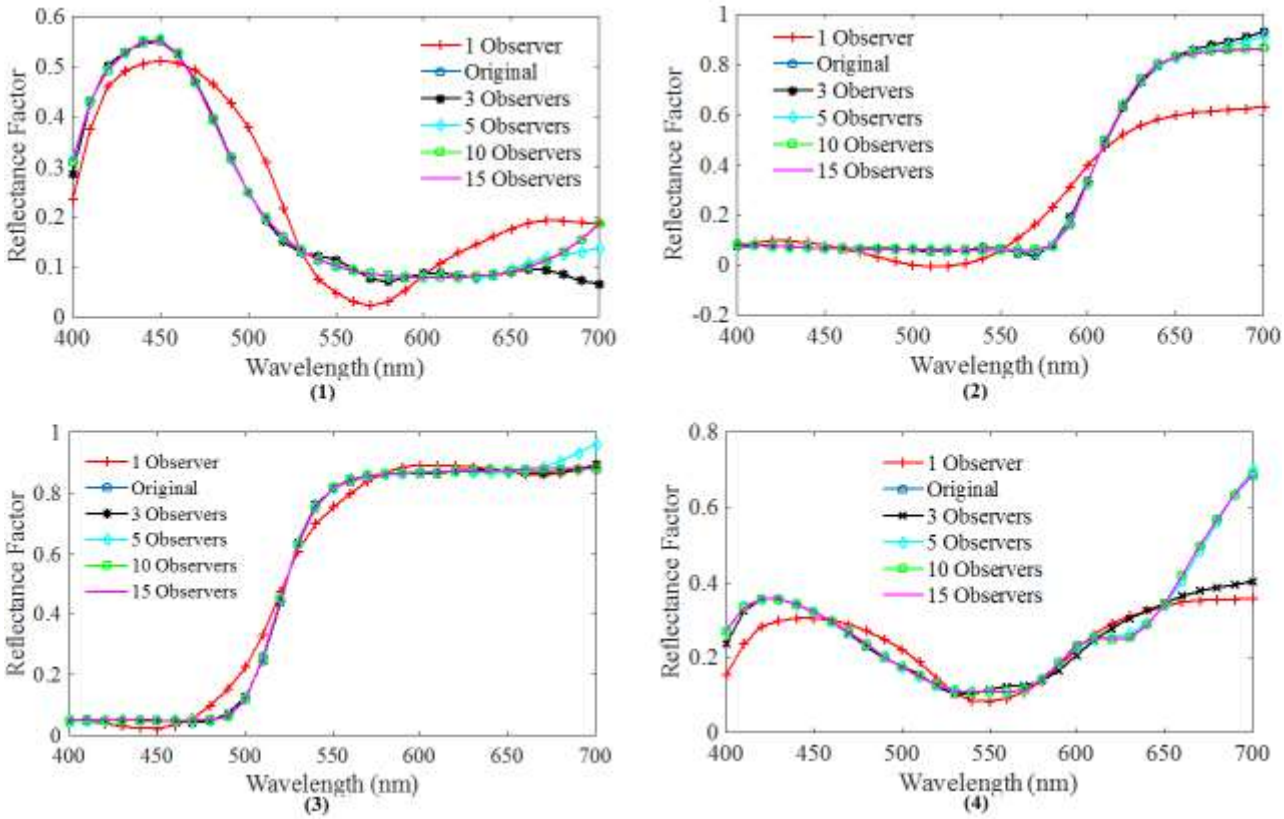

Figure 8. 4 randomly selected samples of testing sample 1.

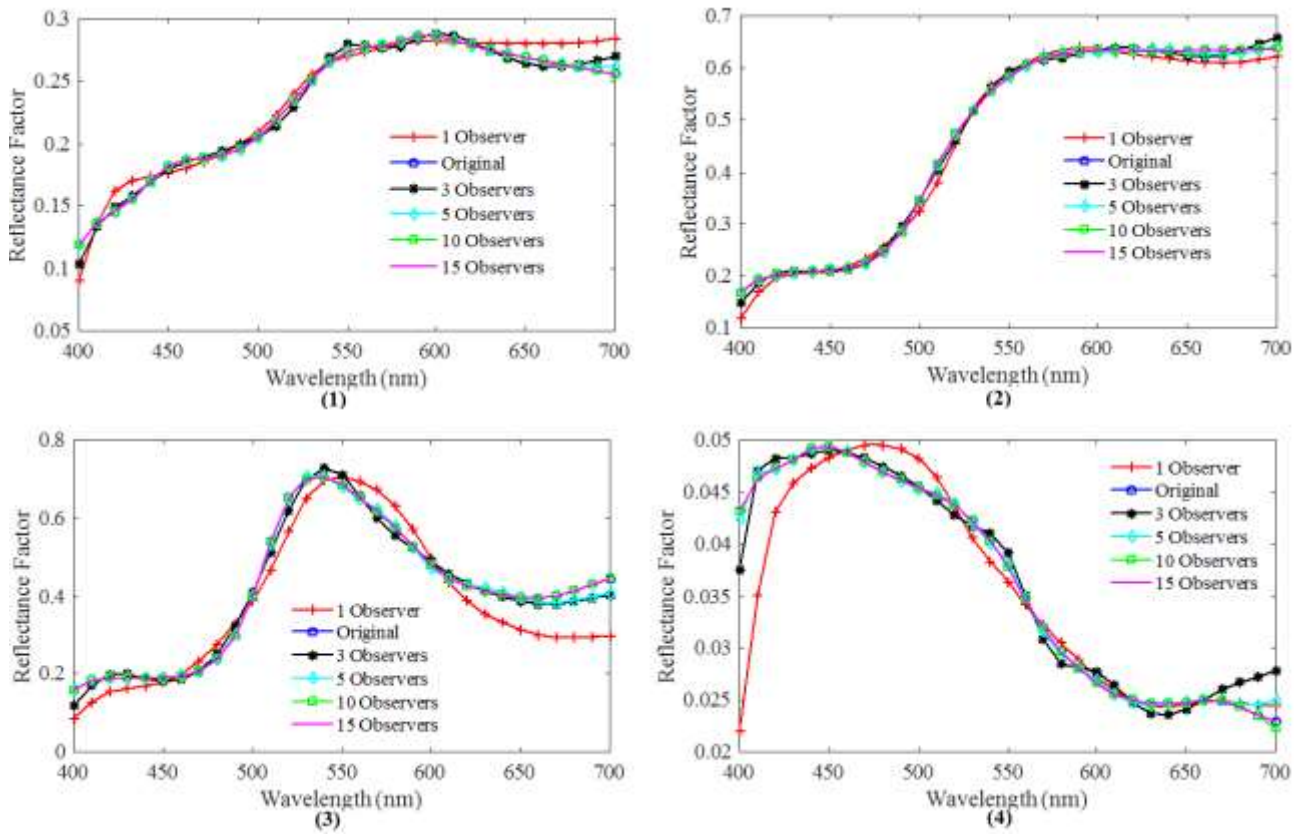

Figure 9. 4 randomly selected samples of testing sample 2.

Looking at Figs. 8 and 9, one would again observe the high accuracy attained utilizing larger number of observers.

4.1.2. Camera

In this part of the thesis, an attempt is made to generalize the idea presented in this work to cameras. In order to test the idea, the cameras' sensitivities presented in Fig.1 are put into use to simulate a situation where the cameras are taking photos of the learning and testing samples; the mean spectral error and color difference results for the two testing samples used in this work are illustrated in Fig.10.

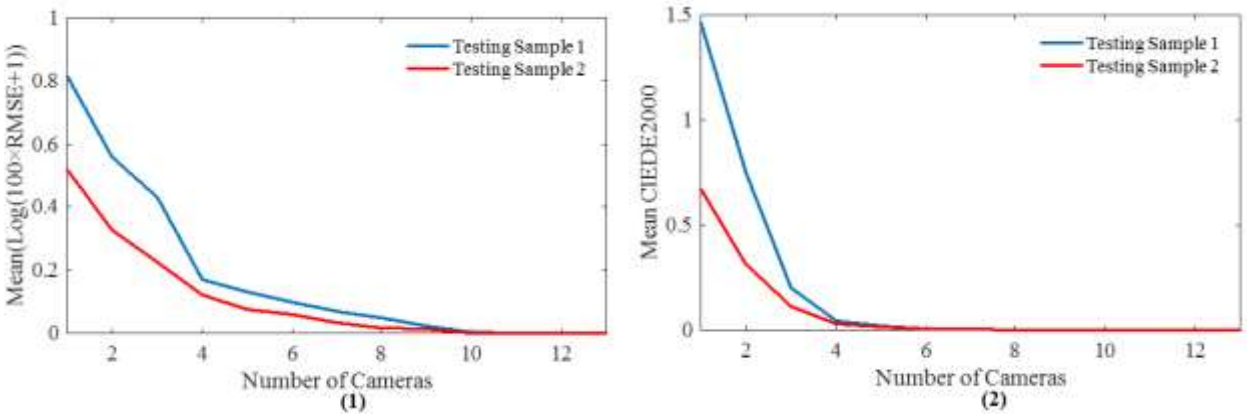

Figure 10, (1): mean spectral error and (2): mean color difference between the original and recovered reflectance spectra of testing samples using different cameras' sensitivity.

As it is observed from Fig.10, again a similar trend of results is elicited from randomly adding more and more cameras and as a consequence adding more RGB data together as in the prior section; in other words, the larger the number of RGB data, the better the recovery precision. It should be noted the discrepancy between the spectral sensitivities is also of fundamental importance. To clarify, if the cameras' sensitivities are different enough from each other (the same as humans in the prior section), the spectral reflectance can be reconstructed in more accurate manner. As it is observed from the Fig. 10, again the error of recovery in the case of the testing sample 1 is larger than the testing sample 2; this fact has to do with the learning samples and how similar or different they are to or from the testing samples. It is obvious from the result of the recovery that testing sample 2 bears a higher level of resemblance to the learning samples than does the testing sample 1 leading to the testing sample 2 having a lower error of recovery.

Looking at Figs. 6 and 10, one would realize that both the camera and observers have resulted in the same trend of results especially after adding 10 sets of spectral sensitivity either from human or camera both have led to the spectral error of zero.

4.2. Practice

4.2.1. Real Camera

This section is split into two subsections of spectral and colorimetric paths. The reason for splitting this section into two more subsections is that the colorimetric error of the recovery is very high when the recovered spectra using real cameras are used for color reproduction as well; therefore, it is aimed to take different paths for colorimetric reproduction as explained below.

4.2.1.1. Spectral Path

The spectral path is further divided into two subsections of random order, in which cameras' and smartphones' responses to the color targets are added randomly together and stepwise, in which first the best camera in terms of spectral recovery is chosen and it continues on to only add the best cameras to this process.

4.2.1.1.1. Random Order

In this section, the camera responses to a specific target would be put together in a random fashion and the spectral recovery error is tracked using the same method as in the prior parts in which the error was shown as the number of added camera or smartphone increased. The results of mean spectral error when random addition of cameras and smartphones is used in spectral reflectance recovery are shown in Figs.11 and 12, respectively. The results of the recovery are shown at the same time for both testing samples; therefore, the same order of randomization of the cameras and smartphones are applied in both cases.

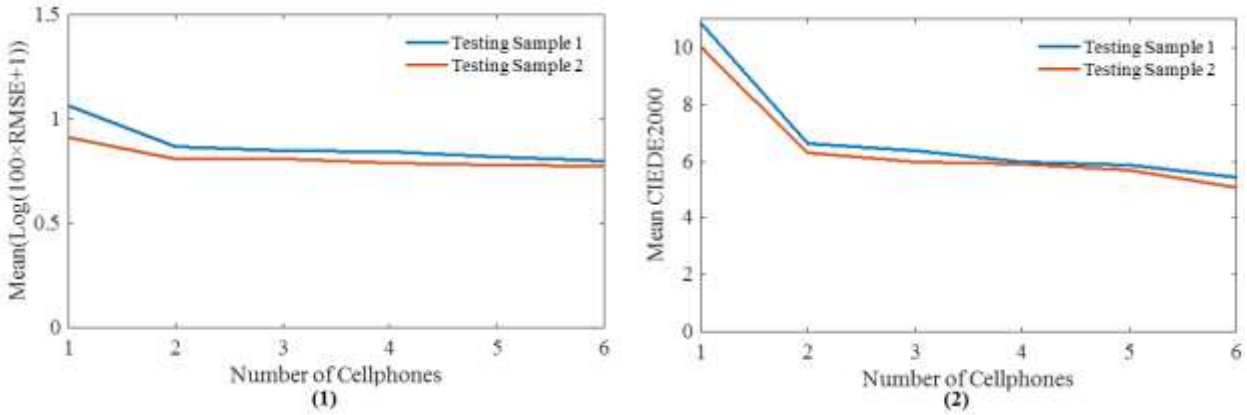

Figure 11. (1): mean spectral error and (2): mean color difference between the original and recovered reflectance spectra of testing samples using different types of smartphones.

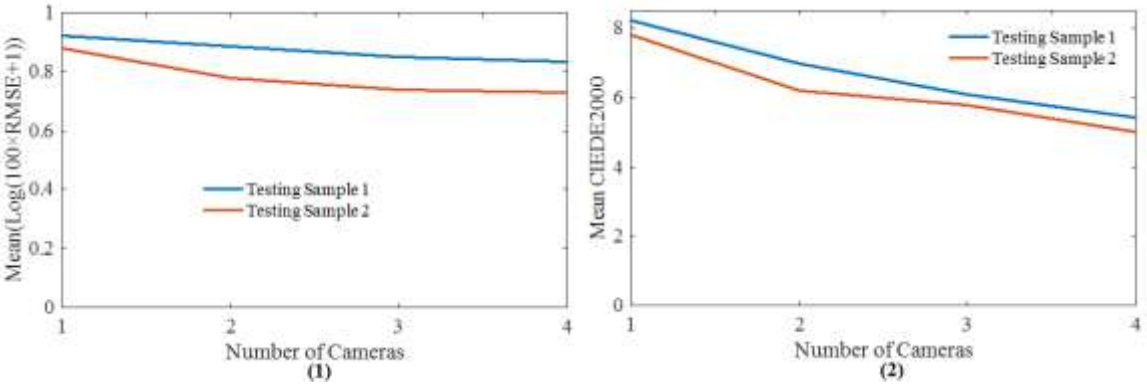

Figure 12. (1): mean spectral error and (2): mean color difference between the original and recovered reflectance spectra of testing samples using different cameras.

As it is observed, again testing sample 2 possesses a lower level of error compared to the testing sample 1, even though the same cameras and smartphones and also the same conditions were applied in both cases; the reason, as mentioned, could be the similarity of the testing sample 2 to the learning samples used in this work. Also, the final results in terms of colorimetric error is still high and not acceptable. The reason why the colorimetric error of recovery is so high even though the corresponding spectral error is very low is not surprising at all. Considering that colorimetric error reports the color difference between the original and the recovered spectra to which the spectral sensitivity of the standard observer has been applied, it would make sense for these two errors not to behave in the same way. In other words, the color difference is calculated between 3 CIELAB values

which are calculated form CIEXYZ tristimulus values; the CIEXYZ have been computed from reflectance spectra of the objects. Therefore, the spectra have been compressed into 3 variables using the spectral sensitivity of the standard observer throwing away all the other information in other parts of the spectrum where standard observer has no sensitivity. However, the error reported in the spectral error recovery is *RMSE* between the two spectra with 31 sampling points across the visible spectrum. Therefore, it is no surprise that these two errors do not act the same, and indeed in the literature use of both errors has been recommended.

4.2.1.1.2. Stepwise Selection

In this section, the cameras are added to the spectral recovery process in a manner that first the best camera is chosen from the cameras available that would be able to lead to the lowest error of recovery (mean spectral error). Then, the second best camera is added; it is chosen in a way that it leads to the lowest possible error among all the others. The process continues until the best cameras in terms of spectral recovery have been chosen in order. In other words, the random order that was used in 4.2.1.1.1 would not be used here but instead cameras are opted for based on how accurate they can recover the spectra. Figure 13 and 14 show the results of the spectral recovery when smartphones and cameras are added in a stepwise manner to the process of spectral recovery from camera response, respectively.

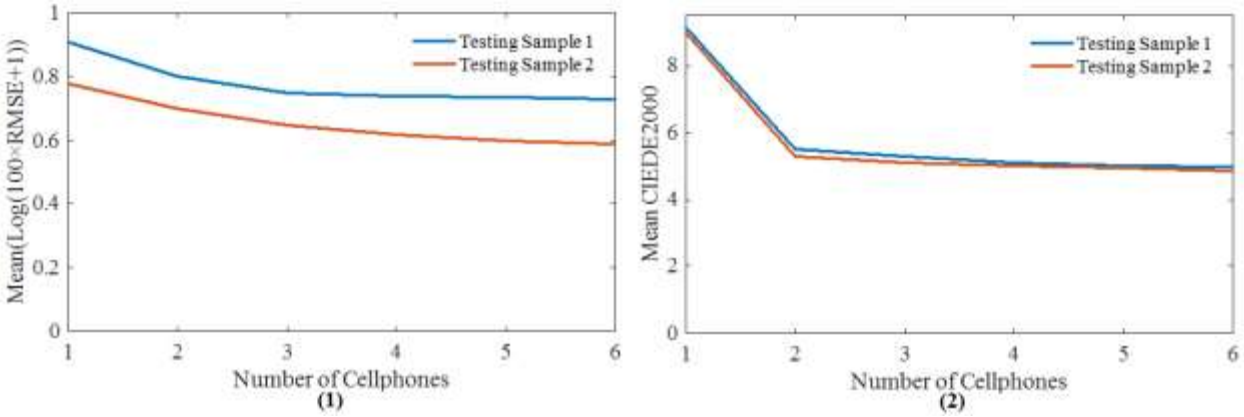

Figure 13. (1): mean spectral error and (2): mean color difference between the original and recovered reflectance spectra of testing samples using different smartphones.

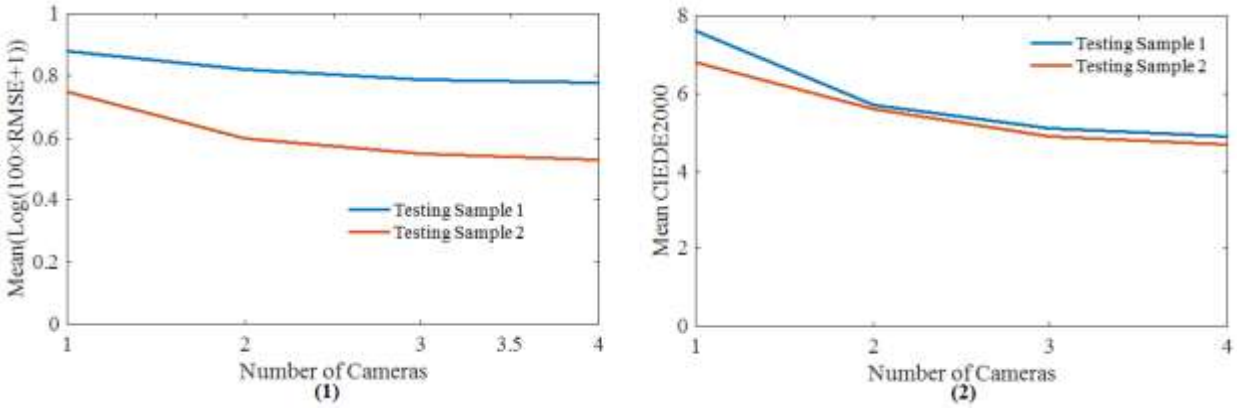

Figure 14. (1): mean spectral error and (2): mean color difference between the original and recovered reflectance spectra of testing samples using different cameras.

As it is observed, the accuracy of the recovery process has increased compared to the case in which the camera responses are added in a random fashion; even though it seems superior to the prior part of the thesis, the method used in this part is of little practical value, in that it looks for the best recovery at first using the testing data to which there is no access in the real situation. However, if there were access to several testing datasets in the real situation, it would be worthwhile going through the same procedure as here making sure that the cameras' responses are being added in the most efficient manner.

4.2.1.1.3. Comparison

Cao et al.'s method would be compared with the method in which several smartphones and cameras were utilized and also to a modified version of the Cao et al.'s method. Additionally, 3 more approaches, namely, weighted pseudo-inverse, nonlinear regression and weighted nonlinear regression, are used. The approaches, as mentioned in Experiment and Procedure are referred to as ran-ph, ran-cam, step-ph, step-cam, Cao, Cao mod, wt-pinv, nonlin, wt-nonlin, respectively. Table 1 illustrates the results of mean *RMSE* and CIEDE2000 when these methods are utilized for recovering the spectra of the testing samples.

Table 1. Results of RMSE and CIEDE2000 between the recovered and original spectra using different methods.

Method	Datasets			
	Testing Sample 1		Testing Sample 2	
	Mean CIEDE2000	Mean RMSE	Mean CIEDE2000	Mean RMSE
ran-ph	5.42	0.058	5.00	0.034
ran-cam	5.45	0.054	5.1	0.050
step-ph	4.9	0.050	4.7	0.024
step-cam	4.97	0.044	4.85	0.029
Cao	5.52	0.049	8.30	0.079
Cao mod	4.23	0.034	4.42	0.042
wt-pinv	3.30	0.025	3.46	0.025
nonlin	3.41	0.029	3.59	0.028
wt-nonlin	2.31	0.021	2.44	0.026

As it is observed from Table 1, Cao et al.'s method has not resulted in a satisfactory outcome, which makes sense considering them regarding RGB camera response as sRGB and changing them to XYZ using the sRGB standard formula. Upon making an alteration

to their approach, in which the RGB camera response was directly emplyed to ccalculate the distance between the testing and training samples (6^{th} method), a significant improvement is observed. The improvement gained using weighted pseudo-inverse, nonlinear regression, and weighted nonlinear regression is also observed in 7^{th}, 8^{th} and 9^{th} method, and comparing them to the their above methods would reveal their superiority. Moreover, using different kinds of cameras and smartphones at the same time seems promising, but not as much as nonlinear regression and the weighted one. In order for these approaches to work in a satisfactory manner, the cameras' spectral sensitivity should be as different as possible; one more point that is worth mentioning is that, using several different cameras at the same time does not allow the hyper-spectral image reconstruction, but using 5^{th} to 9^{th} method would allow this. Obviously, having the spectral reflectance reconstructed at each pixel is more useful than just having the mean spectral reflectance of the surface recovered as done by the 1^{st} to 4^{th} approaches. Weighted nonlinear regression is the best method in terms of accuracy, however, it is also one of the most time consuming methods. Even though the process seems promising using real cameras, there is still a significant colorimetric error needs to be addressed. This significant colorimetric error is indication of several issues, two of the most important ones are the spectral sensitivities of the cameras used and the random noise present in the system. In other words, the spectral sensitivities of the cameras might not be linearly related to the spectral sensitivities of the standard observer resulting in the colorimetric error of the recovery being high. Also, the presence of the noise in the cameras should be kept in mind. Therefore, a separate path is going to be taken to tackle this issue as explained below.

4.2.1.2. Colorimetric Path

In this section, the colorimetric path taken to tackle the problem of high colorimetric error of recovery of the spectral reflectance is expanded upon; one point worth noting is that the process by which the spectra are estimated by putting together different cameras' response is only able to estimate the mean value of the surface spectral reflectance or the colorimetric mean value of the surface. Therefore, it cannot be used to recover the hyper-spectral image in a way that each pixel in the image possesses the spectral information across the visible spectrum. It is not a disadvantage, but it is only a characteristic of the method proposed herein. The colorimetric path enable the reproduction of the color while maintaining the spatial position of the points inside an image; in other words, colorimetric path has two important properties. The first is it can reproduce color more accurately than using the spectral reflectance recovered using the proposed methods herein utilizing the real cameras. The second property of the colorimetric path is it is capable of reproducing a color image under diverse range of illuminants and for any standard colorimetric observers. It should be noted that if it was desired to use several cameras and smartphones for spectral color reproduction in a way that obtaining the recovered image either hyper-spectral or colorimetric one would be doable, the resolution of the cameras should be the same, which was not possible in this work. As it was mentioned in the Experiment and Procedure section of the thesis, there are several types of transforms that are used to transform the camera response (or an RGB image) to a colorimetrically correct image; the transforms include simple pseudo-inverse, pseudo-inverse along with optimization, nonlinear regression and weighted nonlinear regression (consisting of 4 different formulae for calculating the

distance magnitude and weights accrodingly). But in order to do that, there are several other stages that should be undergone, which are explained as follows.

Out of all the cameras and smartphones, first the best one is picked, which is done through looking at the colorimetric accuracy of the cameras and smartphones that were used in the prior sections. In order to do that, first cameras' photometric responses are linearized using the neutral samples of the learning datasets, as explained in the Experiment and Procedure section. For each testing and learning targets, mean patch values are obtained. Then, using simple pseudo-inverse, a matrix of transform is obtained relating the learning samples' RGB response to CIEXYZ values under D65 illuminant for 1964 standard observer. The same matrix is then applied to the testing samples' RGB response to change them to CIEXYZ. The accuracy is then checked in the case of the testing samples. In order to pick the best camera, only the testing sample 1 was used as a criterion. Results of the color reproduction (mean color difference of all the patches between the reproduced CIEXYZ and the original ones) using different types of cameras and smartphones are shown in Table 2. In order to avoid comparing different types of smartphones' and cameras' brands to each other, they are referred to using numbering not their brands.

As it is observed from Table 2, second camera (Nikon D40) has the highest accuracy in terms of color reproduction. Therefore, this camera is chosen as the best one and used in the rest of colorimetric path of color reproduction.

Table 2. Results of color reproduction using different cameras and smartphones.

Camera (and cellphone)	Mean ΔE_{00}
Smartphone 1	4.10
Smartphone 2	4.09
Smartphone 3	4.10
Smartphone 4	4.11
Smartphone 5	4.07
Smartphone 6	4.17
Camera 1	4.07
Camera 2	4.01
Camera 3	4.09
Camera 4	4.05

.

The second stage is to explore the distance and its effect on color reproduction accuracy using the nominated camera. Table 3 shows the effect of distance on mean color difference between original and the reproduced CIEXYZ tristimulus values at different distances.

Table 3. Effect of distance on color reproduction.

Distance	Mean ΔE_{00}
180 cm	4.31
140 cm	4.19
100 cm	3.96
60 cm	4.02

As observed from Table 3, 100 cm is the best place for using this camera; thus, for the future use of this camera in the color reproduction, one woud be better off setting the camera in a way that it is about 100 cm away from the target. Now that we have selected the best camera and specified the distance at which the camera can work more accurately, it is time to try different types of matrix transform to figure out a more accurate and efficient way of transforming the camera response to CIEXYZ. It should be noted that the camera photometric response has already been linearized using the learning samples' neutral patches. Using testing samples 1 and 2, different types of transform approaches from RGB camera to CIEXYZ values under D65 illuminant for 1964 standard observer is tested with results shown in Table 4.

Table 4. Different transform methods used for changing the RGB camera to CIEXYZ under D65 illuminant for 1964 standard observer.

Method	Mean ΔE_{00}	
	Dataset	
	Testing sample 2	Testing sample 1
3×3	3.50	3.96
3×17	3.23	3.08
3×3 Optimization	3.54	3.96
Weighted 3×17 (Euclidean)	1.97	1.88
Weighted 3×17 (Minkowski)	1.85	1.93
Weighted 3×17 (City block)	1.91	1.90
Weighted 3×17 (Chebyshev)	1.99	1.76

The original pictures were taken under light source A in the light booth. As it is observed from Table 4, the linear transform and its optimization possess the worst accuracy in changing the camera RGB response to CIEXYZ values. It might not make sense, since the camera photometric response has been linearized. However, only neutral samples have been used for it and it is assumed that they were able to account for the nonlinearity present in the camera system, but as this table shows there is still some nonlinearity that has been left, leading to nonlinear transform used herein working better than the linear ones. It makes sense for the optimization method to result in a worse result than the linear method itself; because in optimization, the transform matrix is optimized using the learning samples, then the same matrix is applied to testing samples. Obviously, such a matrix that has been fit in this way to learning samples, could lead to a worse result when applied to the testing samples. Nonlinear regression used in this Table, is one of the best approaches, in that it has reduced the error of transform and it has also been very fast and not time-consuming to run. Finally, the weighted nonlinear regression has led to the best accuracy compared to the other methods. This accuracy also makes sense, because in this method testing samples are taken into consideration, and the weights are calculated based on how far testing samples are from the learning ones. Consequently, testing samples having a smaller distance to the learning samples would possess a bigger weight, and the transform matrix is obtained separately for each testing sample taking into accounts these weights. As it is observed, different distance formuluae have led to different outcomes depending on the types of datasets used for testing. In the case of testing sampe 1, Chebyshev has led to the most accurate colorimetric result and in the case of the testing sample 2, Minkowski has resulted in the highest level of colorimetric accuracy. Weighted regression method, on

the other hand, is regarded as costly considering that each testing sample (each pixel) would have its own transform matrix. Therefore, the 3×17 regression method is the most efficient one considering that this method is fast and accurate enough at the same time even though the high accuracy of the weighted regression cannot be ignored. At the end of this section, some visualizations are made for each method to see how different they are when the samples are visualized. In these visualizations, the original pictures are taken under light source A in the light booth, and they are transformed to CIEXYZ under D65 illuminant and for 1964 standard observer. Figure 15 shows the visualization for testing sample 1 (along with the learning sample that is inside the image) and Figure 16 shows the same thing for testing sample 2; in the case of the testing sample 2, a painting is also present in the picture. In the case of the weighted regression, only the result of distance formula having led to the best accuracy are shown.

The proposed procedure here can be used in real situations, where the spectra have been recovered but the colorimetric error is still significant; in other words, the colorimetric path proposed herein can be used and color of the object under different viewing conditions can be simulated with an acceptable level of accuracy, without any need to the spectral reflectance of the object itself, as observed from Figs. 15 and 16.

(1)

(2)

(3)

(4)

(5)

Figure 15. (1): Original picture (2): Pseudo-inverse (3): Optimized Pseudo-inverse (4): Regression and (5): Weighted Regression in the case of testing sample 1.

(1)

(2) (3)

(4) (5)

Figure 16. (1): Original picture (2): Pseudo-inverse (3): Optimized Pseudo-inverse (4): Regression and (5): Weighted Regression in the case of testing sample 2.

4.2.2. Semi-real Human (Regression)

It would be interesting to find out an approach to extend the method suggested herein to a series of current research publications, where authors strive to reconstruct the reflectance spectra from their corresponding colorimetric CIEXYZ tristimulus values.

In the section of Experiment and Procedure, the idea was enlarged on and it was touched upon that one viable method would be to utilize the nonlinear regression. Using this approach, a matrix transform between the XYZ of the simulated observers and the 1964 standard observer is specified. Through utilization of this matrix, the estimation of the simulated observers' response to the testing samples would be possible. The two methods, namely, non-weighted and weighted nonlinear regression, would be compared together herein. Figure 17 illustrates the mean spectral error for these two approaches. It should be noted that the first observer is 1964 standard observer, and the simulated ones would be added to this observer one by one as in prior sections.

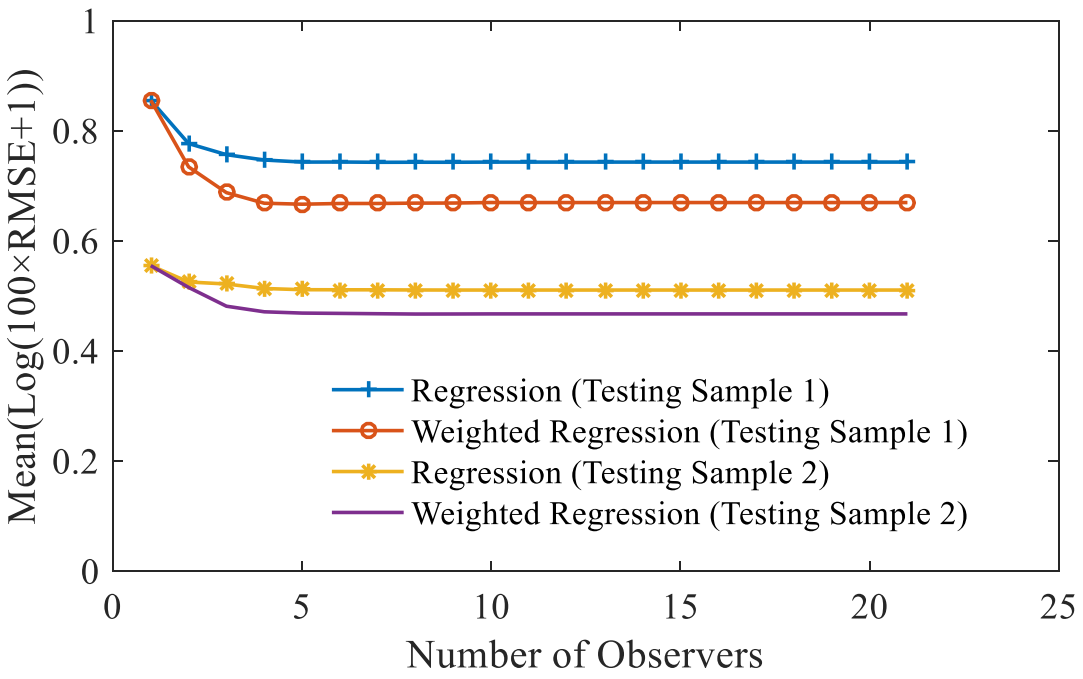

Figure 17. Mean spectral error as the number of observers increases.

As it is observed from Fig.17, the weighted regression has led to a more accurate result that makes sense. Since utilizing weighted regression, the precision with which the XYZ of the simulated observers are estimated could be much higher for the testing samples suggesting that the approach proposed herein for the spectral recovery is viable if the response of the observers can be obtained as precise as possible. Also, as it is observed from Fig.17, in comparison to the results of 4.1.1, the constant line would be reached sooner, and through utilization of smaller number of observers, constant results can be attained. The mean color difference under illuminant A is additionally illustrated in Fig.18.

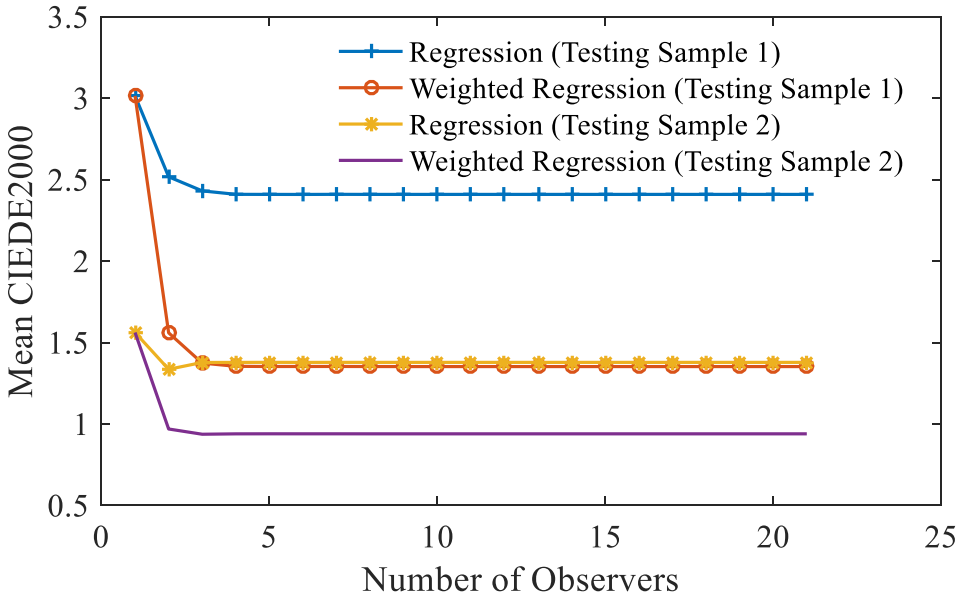

Figure 18. Mean CIEDE2000 as the number of observers increases.

Once again, a similar trend of results is observed here; in other words, the weighted regression has produced better results in comparison to the non-weighted regression. All in all, it is engrossing to note that having access to a larger set of colorimetric data for a specific object could heighten the recovery accuracy of its reflectance. There are a few approaches in order to increase the data dimension, such as using colored filters in front of cameras, or using colorimetric information under diverse range of light sources; in this work, it was shown that utilizing different observers can also be a promising method to do so. One point worth mentioning is that the response of the observers to an object color should be first obtained as accurately as possible; since each observer is holding a particular spectrum part (just like a puzzle) and if the spectral reflectances are to be acquired as accurately as possible, the pieces held by all the observers should indeed be as precise as possible.

At the end of this section, 4 randomly selected specimens of the two testing samples are illustrated in Figs.19 and 20 using different approaches suggested in this section and different number of observers (the number of observers is 1, 3, 5 and 10, since looking at the error, one would realize that after addition of 5 observers, the error is very similar).

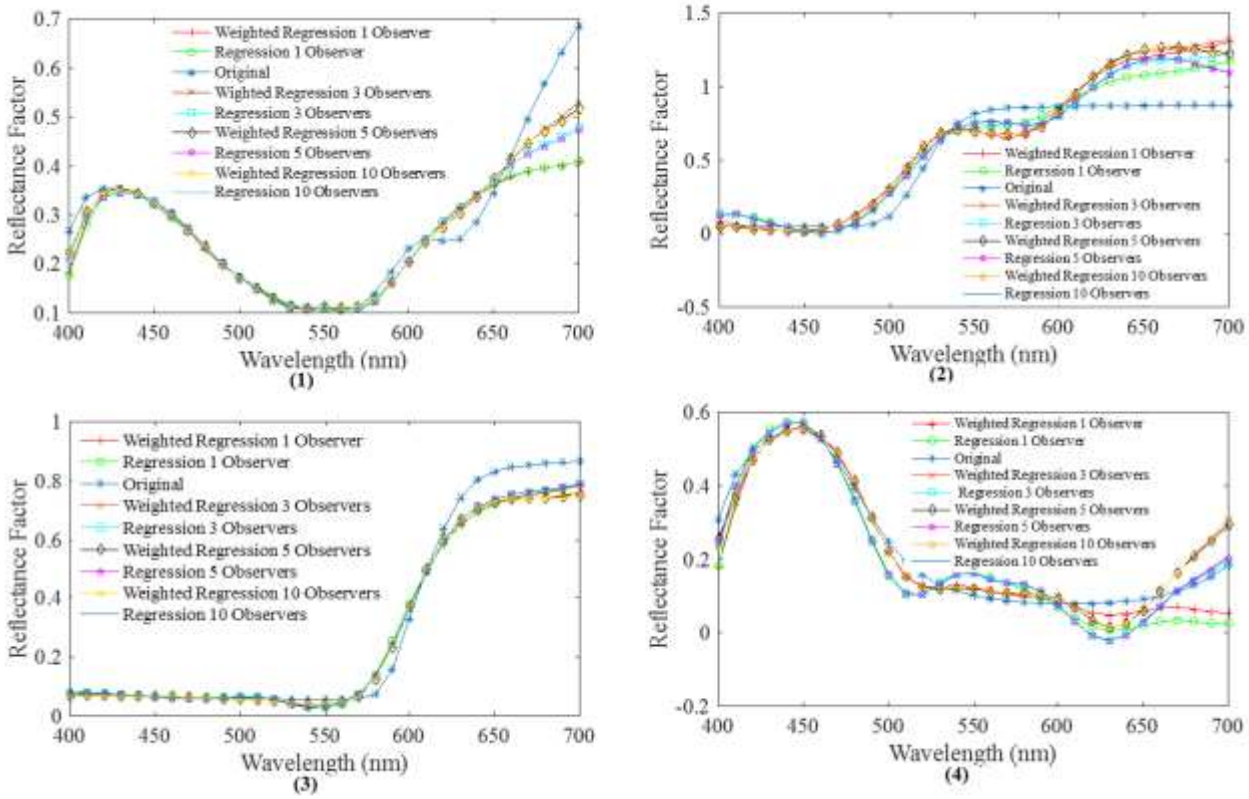

Figure 19. Four randomly selected original and recovered samples of Testing Sample 1 using different number of observers and methods.

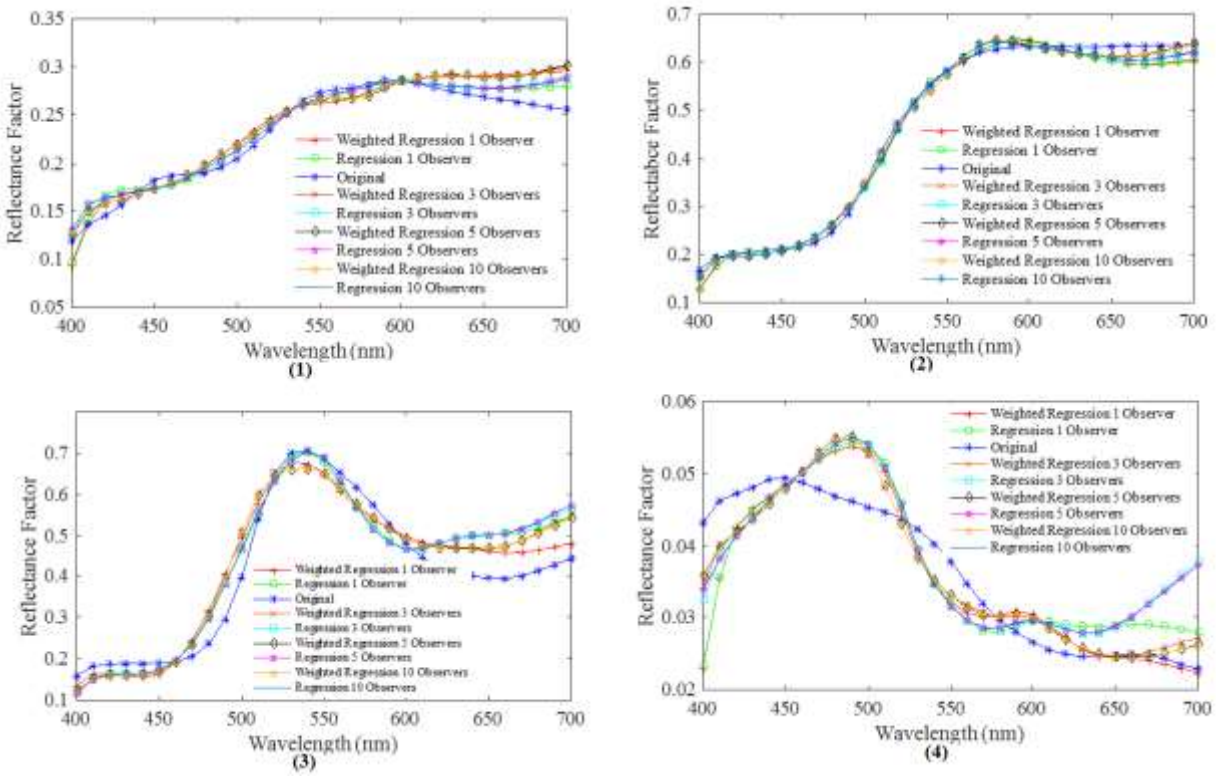

Figure 20. Four randomly selected original and recovered samples of Testing Sample 2 using different number of observers and methods.

As it is observed from Figs. 19 and 20, the weighted regression technique results are better than the regression when a similar number of observers are utilized for both.

4.2.3. Semi-real Human (Color Matching)

Up to now, different approaches were suggested to simulate the response of the observers to a particular stimulus. In this section, yet another method is used to acquire the colorimetric response of the observers which is called color matching.

The same set of simulated observers as in the preceding sections are utilized. Fig.21 illustrates the mean spectral error and also mean color difference between the recovered and the original testing samples as the number of observers increase in two conditions; one with random noise added to the simulated observers' response and one without noise. The

logic behind adding random noise to the observers' response is trying to make the situation more realistic.

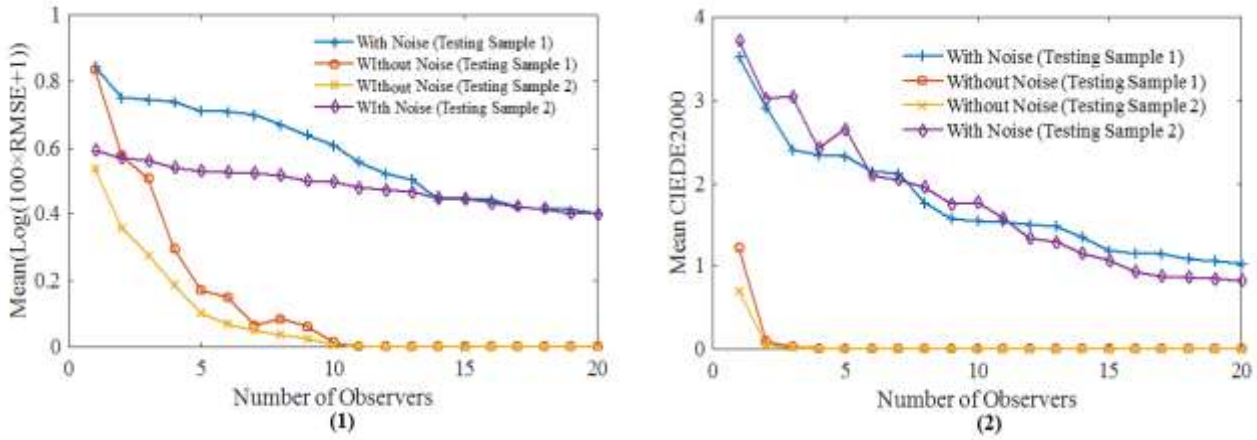

Figure 21, (1): mean spectral error and (2): mean color difference between the original and recovered reflectance spectra of testing samples as the number of observers increases.

As it is observed from Fig.21, the error of the recovery reduces very dramatically subsequent to adding more and more observers to the process; nonetheless, when there is random noise, the error goes on decreasing upon addition of more and more observers. Still an acceptable accuracy level has been reached in this case as well. It is worth noting that using smaller number of observers, testing sample 2 could have a reconstructed reflectance more accurate than the testing sample 1, as mentioned before, showing the greater similarity of this testing sample to the learning set used in this work.

It should be noted that in the case of the cameras and smartphones, real noise can impose a similar limitation to the spectral recovery from the camera response as in this section.

4.3. Multi-Spectral Imaging Camera

At the end of the thesis, a comparison is made between the results obtained using the suggested methods herein with the results using 7 channel multi-spectral camera, which can lead to high accuracy but at a much higher price. The camera is simulated through utilization of 7 filters' spectral transmittance (which were shown in Experiment and Procedure section), which are placed in front of a monochrome sensor.

Table 5 shows the *RMSE* results (*RMSE* with no alterations is reported) when approaches proposed in this thesis are compared with a multi-spectral camera.

In order for the approaches proposed in this study to work in similar manner to a multi-spectral camera, the sensitivities of the cameras should be as distinct as possible, however, the cameras here were 3 Nikon and 1 Canon; considering this problem, still and an acceptable level of accuracy has been attained. Again, looking at table 5, it is obvious that the results of the recovery of testing sample 2 is superior to their counterpart in testing sample 1.

Because only 4 cameras were utilized in this work, justice would not be done to cameras to make a comparison between their results to other approaches in which a larger number of observers and cameras have been used; therefore, it would be interesting to also report the other methods' results when only 4 cameras and observers are used (the first 4 observers and cameras are utilized for all the approaches). Table 6 shows the outcomes of the recovery utilizing methods when only 4 different sets of spectral sensitivity (which can belong either to human or camera) are used.

Table 5. Results of the spectral recovery error using different approaches (Th, C.M, C.M.W.N and W.R stand for theoretical, color matching, color matching with random noise and weighted regression, respectively) for the two testing samples used in this work (TS1 and TS2 stand for testing sample 1 and testing sample 2, respectively).

Number of Observers	Mean *RMSE*
Multi-spectral Camera (TS1)	0.018
6 smartphones (TS1)	0.053
4 cameras (TS1)	0.058
20 Observers (TS1) (Th)	0.000
13 Cameras (TS1) (Th)	0.000
20 Observers (TS1) (C.M)	0.000
20 Observers (TS1) (C.M.W.N)	0.015
20 Observers (TS1) (W.R)	0.036
Multi-spectral Camera (TS2)	0.009
6 smartphones (TS2)	0.050
4 cameras (TS2)	0.044
20 Observers (TS2) (Th)	0.000
13 Cameras (TS2) (Th)	0.000
20 Observers (TS2) (C.M)	0.000
20 Observers (TS2) (C.M.W.N)	0.015
20 Observers (TS2) (W.R)	0.019

Table 6. Results of the spectral recovery error using different approaches (Th, C.M, C.M.W.N and W.R stand for theoretical, color matching, color matching with random noise and weighted regression, respectively) for the two testing samples used in this work (TS1 and TS2 stand for testing sample 1 and testing sample 2, respectively).

Number of Observers	Mean *RMSE*
Multi-spectral Camera (TS1)	0.018
4 smartphones (TS1)	0.060
4 cameras (TS1)	0.058
4 Observers (TS1) (Th)	0.012
4 Cameras (TS1) (Th)	0.005
4 Observers (TS1) (C.M)	0.011
4 Observers (TS1) (C.M.W.N)	0.045
4 Observers (TS1) (W.R)	0.038
Multi-spectral Camera (TS2)	0.009
4 smartphones (TS2)	0.052
4 cameras (TS2)	0.044
4 Observers (TS2) (Th)	0.005
4 Cameras (TS2) (Th)	0.003
4 Observers (TS2) (C.M)	0.005
4 Observers (TS2) (C.M.W.N)	0.025
4 Observers (TS2) (W.R)	0.019

As it is observed from Table 6, now none of approaches has resulted in zero error of recovery, yet high accuracy of methods such as weighted regression and color matching can be witnessed. Smartphones and cameras have the worst recovery error amongst the

other method, but as mentioned before, if the spectral sensitivities of these devices are different enough from each other it will definitely assist in recovering the spectra more accurately. Nonetheless, in this work, the types of the cameras and smartphones available were limited to some specific ones leading to the spectral recovery process not being as precise as anticipated. Also, the presence of random noise in these systems, as mentioned, should be remembered. All in all, the potential of the methods suggested herein can be taken advantage of in the spectral reflectance recovery of objects with a precision level comparable to that of a multi-spectral camera, but much more cost efficient.

5. Conclusions

Main contributions of the present study can be presented as follows:

- Revealing a positive aspect of spectral sensitivity variability among different individuals
- Devising a method for spectral recovery process which is both cost effective and accurate
- Extension of the spectral reconstruction approach to both CIEXYZ standard and RGB nonstandard color spaces
- Coming up with mehods to enhance the colorimetric color reproduction accraucy of ordinary digital cameras

In this work, it was stated that there is a variability in the visual ability of different individuals; although it might hurt color reproduction devices which try to match the color for everyone in a similar manner, this variability could be taken advantage of in spectral recovery process. This could help obtain the spectra in a manner similar to multi-spectral cameras but at a much lower price. In order to do that, different methods were suggested to extract the observers' colorimetric response to a color target. The first method used for extracting indivuduals' response was through the CMFs simulated using Asano et al.'s method. Moreover, color matching and regression were used for the same purpose (simulating the observers' colorimetric response). In all cases, it was ascertained that the larger the number of individuals, the better the recovery accuracy. The same concept was stated to hold for cameras; in other words, cameras, with three spectral sensitivities have the same variability as in humans. Therefore, camera response to color targets were simulated through a set of spectral sensitivities that were attained from an open database.

It was observed that the larger the number of cameras, the better the recovery accuracy. It was then attempted to use real cameras to see if the same trend of results is obtained after adding more and more cameras. It goes without saying that, the same trend was observed in the real situation. Even though spectrally, the error of the recovery seemed to be acceptable in the case of real cameras, there was still a significant colorimetric error needed to be addressed. Therefore, different path, named colorimetric path, was attempted to better reproduce the color of the testing samples under different lighting conditions. Different methods, such as linear and nonlinear regression, weighted regression, and also optimization were used. It was observed that weighted regression led to the best results in terms of the colorimetric accuracy.

References

1. W.S. Stiles, J.M. Burch, “NPL color-matching investigation: final report,” J. Mod. Optic. **6**, 1-26 (1959).

2. Y. Asano, M. D. Fairchild, L. Blondé, Observer variability experiment using a four-primary display and its relationship with physiological factors, 21st Color and Imaging Conference, 6, 171-176 (2013).

3. CIE. Fundamental Chromaticity Diagram with Physiological Axes—Part 1. CIE Publication No170. 2006.

4. R. S. Berns, “Billmeyer and Saltzman’s principles of color technology”, 3rd editon, New York, John Wiley & Sons. 2000.

5. M. D. Fairchild, “Modeling observer metamerism through Monte Carlo simulation”, In: OSA Annual Meeting, Rochester, 126; 1996.

6. M. D. Fairchild and R. L. Heckaman, “Metameric Observers: A Monte Carlo Approach,” In: Color and Imaging Conference. Society for Imaging Science and Technology, **16**, 185–190 (2013).

7. M. D. Fairchild and R. L. Heckaman, “Measuring observer metamerism: The Nimeroff approach,” Color Res. and App. **41**, 115-124 (2016).

8. A. Sarkar and Blondé L, “Colourimetric observer categories and their applications in colour and vision sciences”. In: *CIE Centenary Conference*, (2013).

9. Y. Asano, M. D. Fairchild, L. Blonde, “Individual colorimetric observer model,” PLoS ONE. **11**, 1-19 (2016).

10. V. Babaei, S. H. Amirshahi, and F. Agahian, “Using weighted pseudo-inverse method for reconstruction of reflectance spectra and analyzing the dataset in terms of normality,” Color Res. Appl. **36**, 295-307 (2011).

11. F. Agahian, S. A. Amirshahi, and S. H. Amirshahi, “Reconstruction of reflectance spectra using weighted principal component analysis,” Color Res. Appl. **33,** 360-371 (2008).

12. T. Harifi, S. H. Amirshahi, and F. Agahian, “Recovery of reflectance spectra from colorimetric data using principal component analysis embedded regression technique,” Opt. Rev. **15,** 302-308 (2008).

13. N. Eslahi, S. H. Amirshahi, and F. Agahian, “Recovery of spectral data using weighted canonical correlation regression,” Opt. Rev. **16,** 296-303 (2009).

14. M. M. Amiri, and S. H. Amirshahi, ‘A Step by Step Recovery of Spectral Data from Colorimetric Information’, Journal of Optics, 44, 373-383 (2015).

15. N. Shimano, “Recovery of spectral reflectances of objects being imaged without prior knowledge” IEEE Trans. Image Process **15,** 1848-1856 (2006).

16. N. Shimano, K. Terai, and M. Hironaga, “Recovery of Spectral Reflectances of Objects Being Imaged by Multispectral Cameras,” J. Opt. Soc. Am. A **24,** 3211-3219 (2007).

17. B. G. Kim, J. Han, S. Park, “Spectral reflectivity recovery from the tristimulus values using a hybrid method,” J. Opt. Soc. Am. A **29**, 2612-2621 (2012).

18. H. S. Fairman and M. H. Brill, “The principal component of reflectances” Color Res. Appl. **29,** 104-110 (2004).

19. I. T. Jolliffe: Principal Component Analysis (Springer-Verlag, New York, 2002) Springer Series in Statistics, 2nd Ed.

20. D. Y. Tzeng and R. S. Berns, “A review of principal component analysis and its applications to color technology,” Color Res. Appl. **30,** 84-98 (2005).

21. T. Jaaskelainen, J. Parkkinen, and S. Toyooka, “Vector-subspace model for color representation,” J. Opt. Soc. Am. A **7,** 725-730 (1990).

22. S. Bianco, “Reflectance spectra recovery from tristimulus values by adaptive estimation with metameric shape correction,” J. Opt. Soc. Am. A **27,** 1868-1877 (2010).

23. M. M. Amiri, S. H. Amirshahi, ‘A Hybrid of Weighted Regression and Linear Models for Extraction of Reflectance Spectra from CIEXYZ Tristimulus Values’, Opt. Rev., **21**, 816_825 (2014).

24. S. H. Amirshahi and S. A. Amirshahi, “Adaptive non-negative bases for reconstruction of spectral data from colorimetric information” Opt. Rev. **17,** 562-569 (2010).

25. F. M. Abed, S. H. Amirshahi, and M. M. Abed, “Reconstruction of reflectance data using an interpolation technique,” J. Opt. Soc. Am. A **26,** 613-624 (2009).

26. Y. Zhao and R. S. Berns, “Image-based spectral reflectance reconstruction using the Matrix R method,” Color Res. Appl. **32,** 343-351 (2007).

27. E. M. Valero, J. L. Nieves, S. M. C. Nascimento, K. Amano, and D. H. Foster, “Recovering spectral data from natural scenes with an RGB digital camera,” Color Res. Appl. **32,** 352-360 (2006).

28. M. D. Fairchild and D. R. Wyble, “Mean observer metamerism and the selection of display primaries”, Rochester Institute of Technology, Munsell Color Science Laboratory.

29. B. Cao, N. Liao, Y. Li, H. Cheng, “Improving reflectance reconstruction from tristimulus values by adaptively combining colorimetric and reflectance similarities,” Opt. Eng. doi: 10.1117/1.OE.56.5.053104.

30. B Cao, N. Liao, H. Cheng, “Spectral reflectance reconstruction from RMG images based weighting smaller color difference group,” Color Res. Appl. **42**, 327-332 (2017).

31. B. Cao, N. W. Yang, H. Chen, “Reconstructing spectral reflectance from digital camera through samples selection,” SPIE, Optoelectronic Imaging and Multimedia Technology IV, doi: 10.1117/12.2245278.

32. R. Shrestha, J. Y. Hardeberg, A. Mansouri, “One-shot multi-spectral color imaging with a stereo camera,” SPIE, Digital Photography VII, doi: 10.1117/12.872428.

33. http://www.cis.rit.edu/~dxl5849/projects/camspec/

34. R. S. Berns, “The science of digitizing paintings for color accurate image archives: a review,” J. Imaging Sci. Technol. **45**, 305-325 (2001).